JGR Atmospheres

RESEARCH ARTICLE
10.1029/2023JD038719

Process-Based Intercomparison of Water Isotope-Enabled Models and Reanalysis Nudging Effects

Hayoung Bong[1], Alexandre Cauquoin[1], Atsushi Okazaki[2], Eun-Chul Chang[3], Martin Werner[4], Zhongwang Wei[5], Namgu Yeo[3], and Kei Yoshimura[1,6]

[1]Institute of Industrial Science, The University of Tokyo, Kashiwa, Japan, [2]Department of Global Environment and Disaster Prevention Sciences, Hirosaki University, Hirosaki, Japan, [3]Department of Atmospheric Science, Kongju National University, Kongju, South Korea, [4]Alfred Wegener Institute, Helmholtz Centre for Polar and Marine Sciences, Bremerhaven, Germany, [5]School of Atmospheric Sciences, Sun Yat-sen University, Guangzhou, China, [6]Atmosphere and Ocean Research Institute, The University of Tokyo, Kashiwa, Japan

Abstract The products from the Stable Water Isotope Intercomparison Group, Phase 2, are currently used for numerous studies, allowing water isotope model-data comparisons with various isotope-enabled atmospheric general circulation model (AGCMs) outputs. However, the simulations under this framework were performed using different parameterizations and forcings. Therefore, a uniform experimental design with state-of-the-art AGCMs is required to interpret isotope observations rigorously. Here, we evaluate the outputs from three isotope-enabled numerical models nudged by three different reanalysis products and investigate the ability of the isotope-enabled AGCMs to reproduce the spatial and temporal patterns of water isotopic composition observed at the surface and in the atmospheric airborne water. Through correlation analyses at various spatial and temporal scales, we found that the model's performance depends on the model or reanalysis we use, the observations we compare, and the vertical levels we select. Moreover, we employed the stable isotope mass balance method to conduct decomposition analyses on the ratio of isotopic changes in the atmosphere. Our goal was to elucidate the spread in simulated atmospheric column $\delta^{18}O$, which is influenced by factors such as evaporation, precipitation, and horizontal moisture flux. Satisfying the law of conservation of water isotopes, this budget method is expected to explain various fractionation phenomena in atmospheric meteorological and climatic events. It also aims to highlight the spreads in modeled isotope results among different experiments using multiple models and reanalyses, which are primarily dominated by uncertainties in moisture flux and precipitation, respectively.

Plain Language Summary Our study focuses on surface and atmospheric water isotopes, which are crucial for understanding climate and environmental processes. We assessed the performance of different climate models that simulate water isotopes and compared them to real-world observations. To accomplish this, we employed advanced atmospheric models that include isotopes and subjected them to different input data sets. We discovered that the accuracy of the simulations varied depending on the specific model and data used, as well as the vertical levels considered. By performing correlation analyses at different spatiotemporal scales, we obtained insights into how well the models align with the observed isotopic patterns in both surface and airborne water. Additionally, we utilized a stable isotope mass balance method to examine how various factors, such as evaporation, precipitation, and horizontal moisture flux, influence changes in the isotopic composition of the atmosphere. This method enabled us to identify the sources of uncertainty in the model results. Our research emphasizes the need for a standardized experimental design when studying water isotopes with climate models. By identifying the dominant sources of uncertainty, our findings will prove valuable for scientists from various disciplines and enhance the understanding of simulated future climate and water cycle studies.

Key Points:

- We built a publicly available data set of isotope-enabled nudged simulations from 1979 to 2020, utilizing three models and three reanalyses
- We decomposed atmospheric processes impacting water isotopes, spanning evaporation to precipitation, leading to the first global estimation
- Modeled water isotope spreads due to model and reanalysis choices were dominated by moisture flux and precipitation uncertainties

Supporting Information:

Supporting Information may be found in the online version of this article.

Correspondence to:

H. Bong,
hayoung@iis.u-tokyo.ac.jp

Citation:

Bong, H., Cauquoin, A., Okazaki, A., Chang, E.-C., Werner, M., Wei, Z., et al. (2024). Process-based intercomparison of water isotope-enabled models and reanalysis nudging effects. *Journal of Geophysical Research: Atmospheres*, *129*, e2023JD038719. https://doi.org/10.1029/2023JD038719

Received 17 FEB 2023
Accepted 5 DEC 2023

Author Contributions:

Conceptualization: Hayoung Bong, Kei Yoshimura
Data curation: Hayoung Bong, Alexandre Cauquoin, Atsushi Okazaki
Formal analysis: Hayoung Bong
Funding acquisition: Kei Yoshimura
Investigation: Hayoung Bong
Methodology: Hayoung Bong, Kei Yoshimura
Project Administration: Kei Yoshimura
Software: Hayoung Bong, Alexandre Cauquoin, Atsushi Okazaki, Eun-Chul Chang, Martin Werner, Zhongwang Wei, Namgu Yeo

1. Introduction

As humanity's greenhouse gas emissions have increased, atmospheric temperatures have risen, affecting the Earth's hydrological cycle. The escalation in emissions has changed the amount of water vapor the atmosphere can hold, thereby amplifying uncertainties in climate model simulations due to changes in linear or non-linear feedback processes in different regions. Understanding these uncertainties, which contribute to the spread of modeled variables, is crucial for improving the accuracy and reliability of climate projections. In the wake of climate change, the atmospheric circulation is undergoing significant shifts, making some regions wetter and

Supervision: Kei Yoshimura
Validation: Hayoung Bong, Atsushi Okazaki, Zhongwang Wei
Visualization: Hayoung Bong
Writing – original draft: Hayoung Bong
Writing – review & editing: Alexandre Cauquoin, Zhongwang Wei

others drier, leading to unprecedented weather and climatic phenomena. Such changes necessitate increasingly accurate tools for understanding and prediction.

To shed light on these complexities, stable oxygen and hydrogen isotopes in water ($H_2{}^{16}O$: 99.75%, $HD^{16}O$: 0.02%, $H_2{}^{18}O$: 0.20%, hereafter referred to as water isotopes) serve as a powerful tool for delving into these challenges. They are widely used in hydrological studies to document Earth's climate variability (Craig & Gordon, 1965; Dansgaard, 1964). The water isotopes possess nearly identical chemical properties to their counterparts but differ in mass. This unique feature makes them invaluable for inferring phase changes in environmental conditions, such as evaporation and condensation (Wright et al., 2009). This distinctive characteristic enables researchers to trace the trajectory of atmospheric moisture from its source to its various destinations (Aemisegger et al., 2014; Diekmann et al., 2021; Dütsch et al., 2018; Fiorella et al., 2018; Lewis et al., 2010; Nusbaumer & Noone, 2018; Sodemann et al., 2008). Consequently, extensive efforts have been devoted to measuring these stable water, oxygen, and hydrogen isotopes in a wide range of natural archives such as ice cores (Gkinis et al., 2021), speleothems (Baker et al., 2019), lake and marine sediments (Leng & Marshall, 2004; Westerhold et al., 2020), corals (Thompson et al., 2022), tree ring cellulose (Vitali et al., 2022), and modern water isotope observations (Lacour et al., 2012; Vystavna et al., 2021; Wei et al., 2019; Worden et al., 2006), among others.

The traditional notation for isotopes is denoted by a delta (δ), and it is used to express a small amount of heavy water isotopes in a sample, specifically $H_2{}^{18}O$ and $HD^{16}O$ (where deuterium D is ^2H), which constitute 0.20% and 0.02% of total water, respectively. This notation is expressed in ‰ (per mil) and is calculated using the equation $\delta X = \left(\frac{R_{\text{sample}}}{R_{\text{standard}}} - 1\right) \times 1{,}000$. In this equation, R represents the ratio of heavy to light isotopes; R_{sample} is the isotope ratio in the water sample, and R_{standard} is the isotope ratio in the reference standard, known as Vienna Standard Mean Ocean Water ($D/^1H = 155.76 \pm 0.1$ ppm, $^{18}O/^{16}O = 2005.20 \pm 0.43$ ppm).

Over the decades, efforts have been made to better quantify the processes governing the variations in measured isotope signals (δD, $\delta^{18}O$, and d-excess $= \delta D - 8 \times \delta^{18}O$). A Water isotope-enabled atmospheric general circulation model (AGCM) was initially developed with the groundbreaking work by Joussaume et al. (1984). Subsequent to this, the numerous advanced models have emerged (Blossey et al., 2010; Brady et al., 2019; Brennan et al., 2012; Cauquoin et al., 2019; S. Dee et al., 2015; Hoffmann et al., 1998; Kurita et al., 2011; J. Lee et al., 2007; X. Lee et al., 2012; Mathieu et al., 2002; Moore et al., 2016; Pfahl et al., 2012; Risi et al., 2010; Roche, 2013; Schmidt et al., 2005; Smith et al., 2006; Sturm et al., 2005; Tindall et al., 2009; Yoshimura et al., 2008). These state-of-the-art models simulate three-dimensional spatiotemporal water isotope values with high-frequency integration times, thereby enabling the explanation of global distributions, seasonal variances, and long-term natural variability of heavy water isotopes under various climate scenarios.

Early comparisons of modeled water isotopes examined the performance of present-day and Last Glacial Maximum simulations using GISS and ECHAM models (Hoffmann et al., 2000; Jouzel et al., 2000). Subsequently, a larger comparison effort was undertaken by the Stable Water Isotope Intercomparison Group (SWING) to assess the reliability of simulation results amongst multiple models (Werner et al., 2004). The latest and most commonly used intercomparison simulation data set is the SWING phase 2 (Risi et al., 2012). This data set has supported numerous studies that interpret measured isotope observations or compare those findings with other models (Conroy et al., 2013; S. Dee et al., 2015; Hu et al., 2018; Shi et al., 2022). However, simulations under this framework have not been nudged using consensus reanalysis data sets, and some results were free-running simulations that followed the experiment design for the comparison of Atmospheric Model Intercomparison Project simulations (Gates, 1992). Therefore, it is unclear whether the differences in water isotope values are caused by the choice of model or the choice of nudged reanalysis. This lack of clarity has motivated our research, so we propose a new uniform experimental design with multiple models for a more rigorous intercomparison and precise uncertainty quantification.

One challenge in comparing water isotope models lies in determining the causes of variations in simulation spreads. Different reanalyses for nudging and variations in model structures—such as tracer transport and moist convection schemes—can significantly affect the spread in modeled isotope values. To achieve simulations and analyses for comparison, we first reconstructed the isotopic fractionation processes from 1979 to 2020 using the nudging technique with representative reanalysis fields in the three models. These were run under consistent present-day boundary conditions, such as orbital parameters and greenhouse gases. The model's performance was verified by comparing it with observed water isotope data, and it was evaluated based on regions, seasons,

and variables such as temperature or precipitation that are highly correlated with water isotope values. However, the model's performance in representing water isotopes can be highly dependent on the observation locations used for evaluation. Additionally, it is difficult to quantify the uncertainties associated with the spreads in model simulations for each fractionation process, from evaporation to precipitation.

In light of this, we need to employ quantitative methods for diagnosing differences caused by model structures, water isotope-related physics, and atmospheric circulations. The necessary methodology involves utilizing a mass budget analysis for the heavy water isotopes related to their change rates in the atmosphere. This rate is expressed as "‰/day" and accounts for various decomposed processes in the water cycle, including evaporation, water transport, and precipitation (while considering fractionation effects). Since the numerical models are designed to solve the governing equations and thereby conserve mass, momentum, and energy, we expect the masses of the water isotopes to be conserved. This means that any changes in the distribution of water isotopes can be accounted for within a closed system. Therefore, by applying this methodology to a range of nudging simulations using different models and reanalyses, we not only endeavor to pinpoint the factors leading to a variety of isotope values but also capitalize on the opportunity to quantify uncertainties in fractionation throughout hydrological processes, at the surface and in the atmosphere.

For the first time in our study, we estimated the decomposed isotopic change rates. The global estimation over the past 42 years explains the fractionation imbalance between the evaporation-derived enriching rate (about 2‰/day) and the precipitation-derived depleting rate (about −3‰/day), highlighting the important role of alleviating this imbalance by the enrichment of horizontal moisture flux-derived fractionation (about 1‰/day) in the atmosphere. Through the incorporation of variations in these estimates, a process-based decomposition approach can be employed to quantify uncertainties in water isotope models. Furthermore, the analysis can indicate how far away the water vapor was transported after being evaporated, as determined by the surrounding temperature and humidity conditions in meteorological phenomena on both the synoptic and mesoscale levels. From a long-range perspective, trend analysis can be used to identify which hydrological processes have influenced the isotope ratios in the atmosphere, and by how much some of decomposed processes will likely change in the future.

This study is the first comparison of water isotope models since the SWING2 project, conducted over 10 years ago. In order to advance to the next phase of the modeled isotope comparison, we used updated observation data sets and performed historical, present-day simulations with newer versions of three of the seven models from SWING2. The remainder of this paper is structured as follows: Section 2 describes the experimental design, models adopted, data sets for evaluation, and surface-atmosphere integrated analysis method. Section 3 evaluates the overall performance of the modeled isotope values against various observations, focusing on the surface and vertical distribution. Section 4 quantifies model spreads and their underlying causes in different regions. Lastly, Section 5 summarizes and discusses our findings and insights gained from applying water vapor budgets using isotopic information.

In essence, this study addresses two crucial questions for a precise comparison that has not been previously attempted:

1. How can we validate modeled water isotopes and interpret the discrepancies against observed water isotopes?
2. How do specific hydrological processes affect atmospheric isotopic ratios in simulations where different models or reanalyses are used for nudging?

To explore the answers to these questions, we conducted targeted experiments to test our hypothesis that the choice of model exerts a more significant influence on the uncertainty in water isotope simulations than the use of different reanalyses for forcing, particularly in key water cycle processes such as evaporation, horizontal moisture flux, and precipitation. Our hypothesis, combined with the methods introduced in this study, allows us to systematically assess both the uncertainty of isotope-enabled models and the associated spread in modeled water isotopes.

2. Experimental Design and Method

2.1. Model Description and Data Set

The model characteristics, reanalysis data sets utilized, and observation databases used for evaluating our simulations are summarized in Table 1. We provide a detailed description of these products below.

2.1.1. Isotope-Enabled GCMs: IsoGSM, MIROC5-Iso, and ECHAM5-Wiso

We performed simulations with three isotope-enabled AGCMs and interpolated the results to the lowest horizontal resolution available among our models (T42, approximately 2.8°) to build the intercomparison data set. IsoGSM (Yoshimura et al., 2008) is an isotope-enabled model built from the Scripps Experimental Climate Prediction Center version of the Global Spectral Model (Kanamitsu, Ebisuzaki, et al., 2002; Kanamitsu, Kumar, et al., 2002) developed at the National Centers for Environmental Prediction (NCEP). The surface model is the Noah Land Surface Model (Noah LSM) (Ek et al., 2003), and atmospheric moisture is convected by Relaxed Arakawa-Shubert (Moorthi & Suarez, 1992) in the horizontal spectral grid and vertical sigma coordinate T62L28 resolution. As a major vapor source of the atmosphere, the assigned sea surface water isotopes are set to 0‰ for both $\delta^{18}O$ and δD. The newly incorporated tracer transport scheme in the IsoGSM is the Non-iteration Dimensional-split Semi-Lagrangian (NDSL) proposed by Juang (2007, 2008), and Juang and Hong (2010). The NDSL was implemented in the regional version of the NCEP spectral model (RSM) as documented by Chang and Yoshimura (2015), and we have now utilized it for the first time in the global version, termed IsoGSM-NDSL (hereafter referred to as IsoGSM). The adoption of this advection scheme marks the principal distinction from the previous version, IsoGSM2, which was nudged toward NCEP-R2 (Kanamitsu, Ebisuzaki, et al., 2002; Kanamitsu, Kumar, et al., 2002) without employing NDSL. It alleviates overshooting Fourier sums in the Gibbs phenomenon of the spectral model, removes negative humidity, and transports more vapor in arid and cold spaces, such as Antarctica and high altitudes.

MIROC5-iso (Okazaki & Yoshimura, 2019) is an isotope-enabled atmospheric component of the Model for Interdisciplinary Research on Climate, Earth System Model (MIROC-ESM) (Watanabe et al., 2010) developed by the Japan Agency for Marine-Earth Science and Technology (JAMSTEC) in collaboration with the University of Tokyo and the National Institute for Environmental Studies. The model utilizes the Chikira-Sugiyama cumulus scheme (Chikira, 2004) and the entraining plume model (Chikira & Sugiyama, 2010) for convective parameterization. It also employs a semi-Lagrangian scheme for the tracer advection. Additionally, the land component, known as Minimal Advanced Treatments of Surface Interaction and RunOff (MATSIRO) (Nitta et al., 2014; Takata et al., 2003), from MIROC-ESM is used as the land surface model, and isotope tracers are implemented by Yoshimura et al. (2006). Sea surface and lake water isotopes were constant at 0‰, whereas sea ice $\delta^{18}O$ and δD were constant at 3 and 20‰, respectively (Joussaume & Jouzel, 1993). The model has a resolution of the

Table 1
Model Descriptions, Reanalysis Data Sets, and Observations Used in This Study Are Detailed as Follows: IsoGSM is Nudged by the Japanese 55-Year Reanalysis (JRA55), the National Centers for Environmental Prediction Reanalysis Version 2 (NCEP-R2), and the Fifth Generation European Center for Medium-Range Weather Forecasts Atmospheric Reanalysis (ERA5)

Model	IsoGSM	MIROC5-iso	ECHAM6-wiso
Resolution	T62L28	T42L40	T63L47
Reanalysis for nudging	JRA55, NCEP-R2, ERA5	JRA55	JRA55
Nudging	Spectral nudging	Standard Newtonian relaxation	Spectral nudging
Time integration	Instantaneous	6 hr average	6 hr average
Tracer transport scheme	non-iteration dimensional-split semi-Lagrangian	semi-Lagrangian	semi-Lagrangian
Moist convection	Relaxed Arakawa-Shubert	Chikira-Sugiyama	Tiedtke-Nordeng
Land surface	Noah LSM	MATSIRO	JSBACH
Seawater	$\delta^{18}O = \delta D = 0‰$	$\delta^{18}O = \delta D = 0‰$ lake (0‰) sea ice (3‰)	$\delta^{18}O = \delta D = 0‰$
Water isotope observation			
GNIP	Global Network of Isotopes in Precipitation/Monthly/Surface (1,017 sites, 1979~)		
SWVID	Stable Water Vapor Isotope Database/Hourly/Surface (25 sites, 2003~)		
Antarctic snow	Database of Antarctic snow isotopic composition/Yearly/Surface (794 sites, 1968~)		
TES	Tropospheric Emission Spectrometer/Daily/Vertical (15 levels, 2004–2018)		

Note. Additionally, JRA55 is utilized for nudging across all three models: IsoGSM, MIROC5-iso, and ECHAM6-wiso. To validate the models' performance, water isotope observations in monthly precipitation (GNIP), hourly surface vapor (SWVID), multi-year Database of Antarctic snow isotopic composition, and daily vertical vapor (TES) are utilized.

horizontal spectral triangular truncation T42, approximately 2.8125°, which is the lowest resolution in this model comparison study, and 40 hybrid sigma-pressure coordinate layers (T42L40).

ECHAM6-wiso is the isotopic version of ECHAM6 (Stevens et al., 2013), the sixth generation of the AGCM ECHAM developed at the Max Planck Institute for Meteorology. It features a dry spectral-transform dynamical core (Simmons et al., 1989), a transport model for scalar quantities other than temperature and surface pressure, and a suite of physical parameterizations to represent diabatic processes (Stevens et al., 2013, and references therein). It also employs Tiedtke's (1989) convective parameterization, which is supplemented by Nordeng's (1994) modifications for deep convection. We used the last version of the ECHAM6-wiso, updated by Cauquoin and Werner (2021), at a spectral resolution of T63L47 (approximately 1.875° horizontal resolution and 47 vertical levels).

2.1.2. Reanalysis Products for Nudging Simulations: JRA55, NCEP-R2, and ERA5

The Japanese 55-year reanalysis (JRA55) is the second global reanalysis version of the Japan Meteorological Agency. The 6-hourly data set covers the last half century since 1958, when radiosondes started to observe the atmosphere regularly. Significant improvements compared to JRA25 (Onogi et al., 2007) were realized by variational data assimilation from 3D-Var to 4D-Var, variational bias correction (Derber & Wu, 1998) for satellite radiances (D. P. Dee & Uppala, 2009), and incorporating more observational data sets. These were obtained from METEOSAT and GMS data, snow depth over the United States (UCAR), Russia (RIHMI), and Mongolia (IMH), introducing time-varying concentrations of greenhouse gases, high spatial resolution, TL319, and vertical levels from L40 to L60 up to 0.1 hPa (Kobayashi et al., 2015).

The National Centers for Environmental Prediction-Department of Energy (NCEP-DOE) Atmospheric Model Intercomparison Project (AMIP-II) reanalysis II (R2) was conducted by the mission of the National Energy Research Scientific Computing Center (NERSC). It is an improved version of NCEP-NCAR Reanalysis I (R1), covering the period from 1948. Compared with the R1 version, R2 has a fixed physical parameterization, better data assimilation, and a planetary boundary layer scheme for nonlocal diffusion. However, R2 only covered the satellite era since 1979. Observations, including satellite temperature retrievals and simulation at the resolution of T62L28, were the same for both data sets (Kanamitsu, Ebisuzaki, et al., 2002; Kanamitsu, Kumar, et al., 2002).

ECMWF Reanalysis (ERA) has a series of data sets, ERA-15, ERA-interim, ERA-40, and fifth generation (ERA5), in chronological order. The latest production, ERA5, achieved finer resolutions: horizontally at 31 km, vertically 137 levels up to 0.01 hPa, and an hourly time resolution (Hersbach et al., 2020). It spans a broader period (1950-present) compared to ERA-interim (1979-August 2019). Moreover, ERA5 adopted the Integrated Forecasting System (IFS Cy41r2) as its operational system in 2016, which is advantageous for examining recent advancements in data assimilation (ECMWF, 2016a), model dynamics (ECMWF, 2016b), and model physics (ECMWF, 2016c).

2.1.3. Water Isotope Observational Products and Climate Data Sets: GNIP, SWVID, Antarctic Snow, TES, CRU TS, and GPCP

The observation data sets used to evaluate the model results consisted of precipitation, snow, and water vapor measurements near the surface and atmosphere. The Global Network of Isotopes in Precipitation (GNIP) measures water isotopes globally every month (IAEA/WMO, 2006). For this study, we utilized a part of 1,017 stations by selecting the sites where measurements had been taken for at least 12 consecutive months from 1979 to 2020. Seasonality was removed from the regional correlation analysis. The Stable Water Vapor Isotope Database (SWVID) was also used for near-surface isotope observations (Wei et al., 2019). This data set gathers isotope measurements made via infrared isotopic spectroscopy over the land surface and sea surface via ship and in the free troposphere via aircraft. The time resolution of the raw data is hourly. We converted these data to daily timesteps using an amount-weighted average for our analyses. To evaluate our simulations for the Antarctic area, we used the Database of Antarctic snow isotopic composition (Masson-Delmotte et al., 2008). The data set includes 1,279 data points: 1,125 locations for $\delta^{18}O$, 938 sites for δD, and 794 sites with data for both isotopes, enabling the calculation of the deuterium excess.

For the atmospheric variables, we compared our simulations with water isotope satellite data for water vapor isotopes in the atmosphere, as explained in Worden et al. (2006). This data is included in the Tropospheric Emission Spectrometer (TES-NASA)/Aura Level 3 Water Vapor Daily Gridded Version 5 data set. It has 15

vertical levels, and this study considers three layers at 825.4, 681.29, and 464.16 hPa, known as the most sensitive levels for estimating the TES δD profile (Yoshimura et al., 2011). The modeled target variables (water vapor and its δD) were interpolated to the TES grids for model-data comparisons (three layers on the vertical, $4° \times 2°$ grid on the horizontal). To remove the impacts of cloudiness (clear-sky bias) induced by poor estimation from the space-borne infrared sensor, all simulations and TES data sets were vertically filtered to remove rainy days according to the Global Precipitation Climatology Project (GPCP) v1.3 Daily Precipitation Analysis Climate Data Record (Adler et al., 2017). The TES data covers the period from 2004 to 2018. However, we note that 2008 was excluded from the analysis due to weak spatial data coverage. Additionally, because of the "Sun Synchronous Orbit" of the TES satellite, there are deficiencies in the water vapor isotope data set at 2-day intervals.

To evaluate modeled temperature and precipitation, which significantly affect isotope values, we used the climate data sets: the Climatic Research Unit's gridded Time Series (CRU TS) v4.06 for near-surface temperature (Harris et al., 2020), supported by an extensive network of weather station observations, and the GPCP v2.3 monthly satellite-gauge combined precipitation (Adler et al., 2016), which integrates satellite precipitation estimates from passive microwave and infrared, along with other low Earth orbit data and in-situ observations.

2.2. Experimental Design and Nudging

Simulated water isotopes differ depending on the models or the forcing conditions employed. Thus, two sets of model simulations were designed to make a rigorous comparison of the water isotope-enabled models. One uses a single reanalysis (JRA55) to nudge the different models (IsoGSM, MIROC5-iso, ECHAM6-wiso), and the other uses a single model (IsoGSM) nudged with different reanalyses (JRA55, NCEP-R2, ERA5). Using these two sets of experiments—Group 1 (IsoGSM.JRA55, MIROC5-iso.JRA55, ECHAM6-wiso.JRA55), which uses a single reanalysis to nudge three models, and Group 2 (IsoGSM.JRA55, IsoGSM.NCEP-R2, IsoGSM.ERA5), which uses multiple reanalyses to nudge one model—it is possible to separately diagnose (a) differences in model physics, and (b) differences in how the reanalysis product applied affects atmospheric dynamics. For nudging simulations, our water isotope-enabled models were nudged toward the chosen reanalysis data considering 3D-fields of temperature (for GSM and ECHAM, except MIROC) and atmospheric circulation (GSM and MIROC: zonal and meridional wind fields; ECHAM: vorticity and divergence), every 6 hr for our period of interest. However, humidity reanalysis data were not utilized for nudging during the simulation of water isotopes. Consequently, while the water isotopes were modeled based on reanalysis circulation information, the humidity in the simulations may vary due to the distinct schemes of each model, even though all three models were nudged by the same reanalysis circulation for the Group 1 experiment. Typically, it takes up to a 1-month model period to reconstruct a reliable atmospheric distribution of water vapor isotopes, regardless of the initial conditions. The sea surface temperature and sea ice fields (GSM: daily mean, MIROC: 6-hourly, ECHAM: monthly mean) from the corresponding reanalysis data set were applied as sea surface conditions for all our experiments.

2.3. Isotope Mass Budget Analysis

This study introduces a new methodology, water isotopic change rates, to quantitatively decompose all transformations of the water isotope ratios in meteoric water. This method quantifies isotope value changes in the atmosphere by considering the gradient of isotope values between the atmospheric column and the surroundings with a weighting amount of water exchange. First, the atmospheric water balance equation describes the change in the water amount (Oki et al., 1995; Väisänen, 1961).

$$\frac{\partial W}{\partial t} = E - P - \nabla \cdot \overrightarrow{Q} \left[\mathrm{kg/m^2/s}\right] \tag{1}$$

W, $\overrightarrow{Q}$, $\nabla \cdot \overrightarrow{Q}$, E, and P represent the following quantities: W is the precipitable water in a column (which refers to the water abundance per unit square meter); $\overrightarrow{Q}$ is the vertically integrated horizontal moisture flux vector; $\nabla \cdot \overrightarrow{Q}$ denotes the horizontal moisture flux divergence, which describes the rate of vapor spreading out from a point per unit square meter. Positive values indicate that more moisture is leaving an area than entering, leading to drying, whereas negative values mean more moisture is entering than leaving, causing moistening; E stands

for evaporation flux, and P refers to the precipitable flux. The horizontal moisture flux divergence can be decomposed into the following equations:

$$Q_\lambda \equiv \int_0^{P_0} qu\frac{dp}{g}\ [\mathrm{kg/m/s}] \tag{2}$$

$$Q_\phi \equiv \int_0^{P_0} qv\frac{dp}{g}\ [\mathrm{kg/m/s}] \tag{3}$$

$$W \equiv \int_0^{P_0} q\frac{dp}{g}\ [\mathrm{kg/m^2}] \tag{4}$$

$$\nabla\cdot\overrightarrow{Q} = \frac{1}{R_e\cos\phi}\left(\frac{\partial Q_\lambda}{\partial\lambda} + \frac{\partial Q_\phi\cos\phi}{\partial\phi}\right)[\mathrm{kg/m^2/s}] \tag{5}$$

Here, $\overrightarrow{Q} = (Q_\lambda, Q_\phi)$ represents the zonal (longitude, λ) and meridional (latitude, ϕ, where $\cos\phi = 1$ at the equator) components of the moisture flux vector. $\frac{\partial Q_\lambda}{\partial\lambda}$ and $\frac{\partial Q_\phi\cos\phi}{\partial\phi}$ are the rates of change of the zonal and meridional components of $\overrightarrow{Q}$ with respect to longitude and latitude, respectively. R_e is the equatorial radius. Changes in precipitable water in the atmosphere (W) are determined by the inflow and outflow of moisture flux over a specific time interval ($\Delta t = 6\,\mathrm{hr}, 6\times60\times60\,\mathrm{s}$):

$$\begin{aligned} W_{t+\Delta t} - W_t &= \Delta W_{t\to t+\Delta t} \\ &= (E_t - P_t + F_{\mathrm{in}t} - F_{\mathrm{out}t})\Delta t\ [\mathrm{kg/m^2}] \end{aligned} \tag{6}$$

where F_{in} and F_{out} are the horizontal incoming and outgoing moisture flux components in the convergence, respectively. Second, the water balance equation for the gradient of isotope values is multiplied by the surrounding isotope ratios (δe_t, δp_t, $\delta q_{\mathrm{in}t}$, and $\delta q_{\mathrm{out}t}$) accompanying the water exchange to approximate the isotopic mass balance form in Equation 7 (Hayes, 2004; Yoshimura et al., 2003), and the isotope ratio in the column in Equation 8. In this study, δw refers to the oxygen isotope value in the vertically mass-weighted sum of the water vapor in the atmosphere.

$$W_{t+\Delta t}\delta w_{t+\Delta t} - W_t\delta w_t = (E_t\delta e_t - P_t\delta p_t + F_{\mathrm{in}t}\delta q_{\mathrm{in}t} - F_{\mathrm{out}t}\delta q_{\mathrm{out}t})\Delta t[‰]\ [\mathrm{kg/m^2}] \tag{7}$$

$$W_{t+\Delta t}\delta w_t - W_t\delta w_t = (E_t\delta w_t - P_t\delta w_t + F_{\mathrm{in}t}\delta w_t - F_{\mathrm{out}t}\delta w_t)\Delta t\,[‰]\ [\mathrm{kg/m^2}] \tag{8}$$

where δe_t, δp_t, $\delta q_{\mathrm{in}t}$, $\delta q_{\mathrm{out}t}$ are isotope values in evaporation, precipitation, and the ambient isotope ratio of oxygen entering and exiting through horizontal moisture flux, respectively. By re-organizing Equations 7 and 8 (Krabbenhoft et al., 1990), we defined $\Delta\delta w_t$, isotopic change rate in a column as follows:

$$\begin{aligned} \frac{\delta w_{t+\Delta t} - \delta w_t}{\Delta t} &= \Delta\delta w_t \\ &= \frac{E_t(\delta e_t - \delta w_t) - P_t(\delta p_t - \delta w_t) + F_{\mathrm{in}t}(\delta q_{\mathrm{in}t} - \delta w_t) - F_{\mathrm{out}t}(\delta q_{\mathrm{out}t} - \delta w_t)}{W_t + \left(E_t - P_t - \nabla\cdot\overrightarrow{Q_t}\right)\Delta t} \\ &= \Delta\delta w_{e_t} + \Delta\delta w_{p_t} + \Delta\delta w_{q_t}\ [‰/\mathrm{s}] \end{aligned} \tag{9}$$

where $\Delta\delta w_e$, $\Delta\delta w_p$, $\Delta\delta w_q$ are the isotopic change rates derived from the evaporation, precipitation, and horizontal moisture flux, respectively.

Please note that water amounts (E_t, P_t, $F_{\mathrm{in}t}$, and $F_{\mathrm{out}t}$) are weighted to the gradients between ambient water isotope values (δe_t, δp_t, $\delta q_{\mathrm{in}t}$, and $\delta q_{\mathrm{out}t}$) and column value, δw_t. These weighted gradients are further adjusted by current precipitable water (W_t) and change in water amount, $\left(E_t - P_t - \nabla\cdot\overrightarrow{Q_t}\right)\Delta t$ ($[\mathrm{kg/m^2/s}] * [\mathrm{s}] = [\mathrm{kg/m^2}]$), while the column isotope value (δw_t) evolves to the next time-step value ($\delta w_{t+\Delta t}$) over a time interval Δt, assuming the frac-

tionation factors for each process are constant during 6 hr. However, during our preliminary testing prior to fully adopting the method, we confirmed that the conservation of mass for water isotopes becomes less reliable as the time interval expands, due to the inability to account for changes in the fractionation factor over extended periods. This limitation presents challenges for validation against low-time-resolution satellite water vapor isotope data sets, as the isotopic change rate (‰/s) is currently only calculable through isotope-enabled models.

As we assumed in this study that water and heavy water isotope masses are conserved, we can define contributions to $\Delta\delta w$ in the following manner:

$$C_{\delta X_t} = \frac{|\Delta\delta w_{X_t}|}{|\Delta\delta w_{e_t}| + |\Delta\delta w_{p_t}| + |\Delta\delta w_{q_t}|} \times 100\,(\%) \tag{10}$$

where $C_{\delta e}$, $C_{\delta p}$, and $C_{\delta q}$ (instead of $C_{\delta X}$) are the relative contributions of evaporation ($\Delta\delta w_e$), precipitation ($\Delta\delta w_p$), and horizontal moisture flux ($\Delta\delta w_q$), respectively, to the total isotopic change rate in a column, $\Delta\delta w$. This method takes absolute values to consider all processes, regardless of enrichment or depletion of water isotopes (see Text S1: Method details in Supporting Information S1).

3. Results: Evaluation of Modeled Water Isotopes

3.1. Surface Variables

3.1.1. Mean Conditions and Global Distribution of Water Isotopes

The annual mean of model ensembles of Group 1—three models nudged toward JRA55—presents temperature (Figure 1a), precipitation (Figure 1b), evaporation (Figure 1c), and near-surface humidity (Figure 1d). Figures 1e–1h illustrate their variables' spread in the models. When constraining sea surface temperature and sea ice concentration to a single reanalysis, simulations over the ocean exhibit a significantly smaller surface temperature spread (as indicated by the standard deviation of Group 1) compared to the land (Figure 1e). On the land surface, even when the same atmospheric temperature and circulation are applied to the models (except for MIROC5, which differs with respect to nudging vertical temperature), the different land components of the three models can cause variations in radiative energy and moisture exchange. This can enlarge the spread of modeled skin temperature. Particularly in Antarctica, where the spread of modeled temperature is most prominent, various model schemes for cloud physics and snow and resolutions (Tewari et al., 2022), which affect the topography in the models, could induce different temperatures due to the different reflections of incoming solar radiation and outgoing ocean thermal radiation.

Precipitation spread is most noticeable in the tropics (Figure 1f), where warm surface conditions trigger uplifting air and maintain low-level convergence. One possible cause may be the different moist convection schemes influencing cloud formation. Another factor could be the different strengths of nudging among the models. These differences result in different low-level moisture convergences for precipitation, especially in the Intertropical Convergence Zone (ITCZ). Such differences in model characteristics amplify the spread of rainfall and the depth of convective clouds in the subtropical North and South Pacific and Atlantic. Moreover, land models and monsoons can impact the spread of precipitation in Amazonia and even more significantly in Central Africa. This is because the Atlantic and Indian oceans supply differing amounts of water vapor depending on the season.

In the Amazonia and Central Africa regions, the amount of evaporation varies depending on the model considered (Figure 1g). Meanwhile, processes like evapotranspiration from plants and re-evaporation from the soil, which influence moisture flux release into the atmosphere, are defined differently across our models. IsoGSM and ECHAM6-wiso do not account for fractionation processes during evaporation over the land surface, whereas MIROC5-iso incorporates kinetic fractionation for surface water evaporation. Over the ocean surface, the modeled surface moisture and drag coefficient may contribute to the spread of evaporation, but they are much smaller contributors compared to the spread of precipitation.

The spread of surface layer humidity, or the humidity in the bottom-most layer of the atmosphere in a hybrid sigma-pressure vertical coordinate (Figure 1h), can be explained by multiple spreads of other variables (as shown

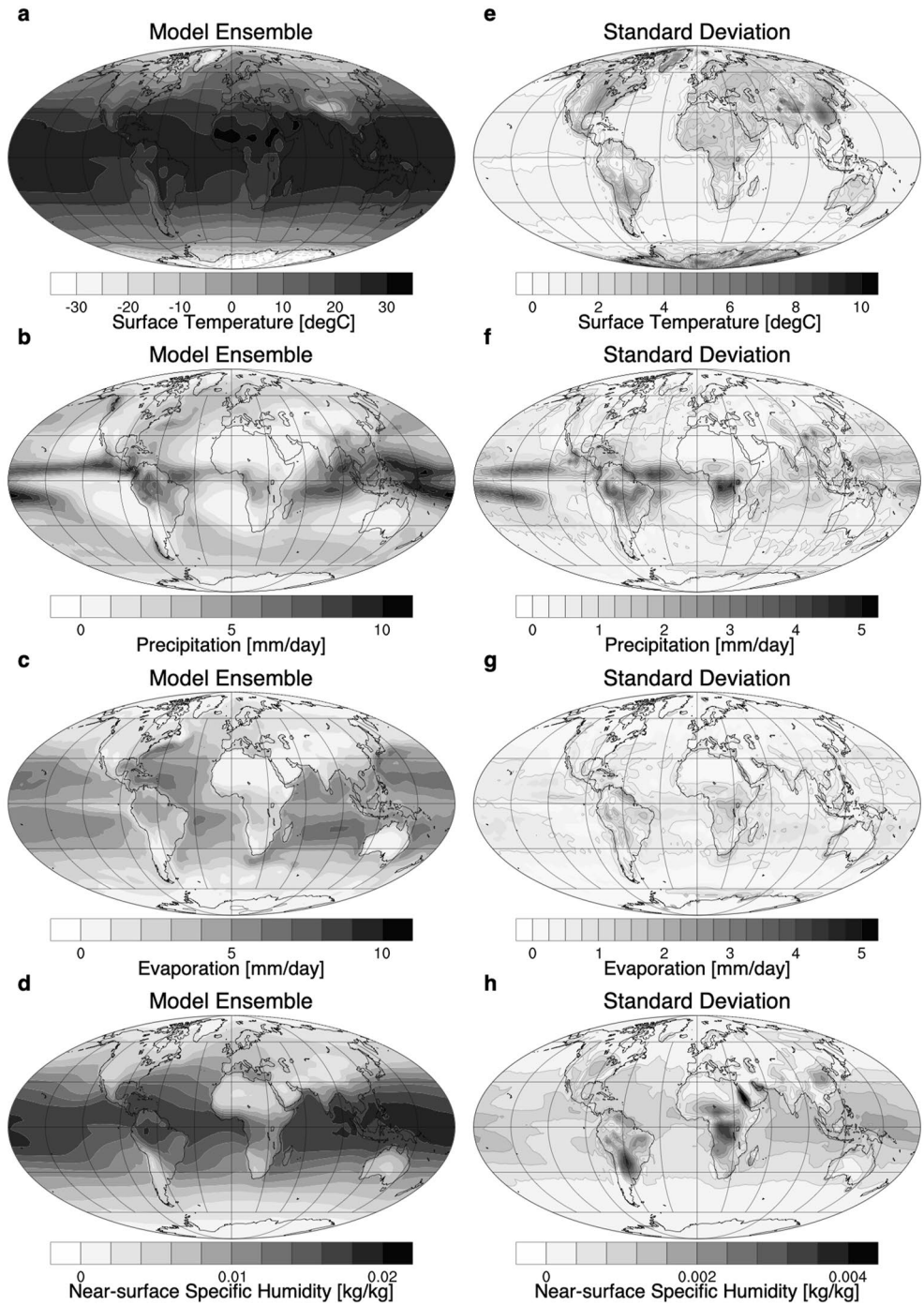

Figure 1. The annual mean of model ensemble (a–d), which averages three models from Group 1: IsoGSM.JRA55, MIROC5-iso.JRA55, ECHAM6-wiso.JRA55. Additionally, the standard deviations for each ensemble are shown in figures (e–h). These are for the following variables: (a, e) surface temperature (°C), (b, f) total precipitation (mm/day), (c, g) surface evaporation (mm/day), and (d, h) near-surface specific humidity (kg/kg), respectively.

in Figures 1e–1g). Since precipitation moistens soil, the spread of modeled surface humidity in Central Africa correlates with the spread of rainfall. However, the spreads of modeled temperature, which arise from the different land schemes in the grasslands east of the Andes Mountains, can increase the range of water vapor the near-surface air can contain. As a result, these spread patterns in four key variables (temperature, precipitation, evaporation, and near-surface humidity) play a role in explaining the differences in modeled surface water

content, vapor distribution, and snow cover among different models. This variability in modeled outcomes can be largely attributed to model uncertainty in simulating the water cycle.

When investigating the disparities in the modeled water cycle, examining arid regions such as deserts or high-latitude areas has limitations in measuring these spreads of modeled water amounts at the surface (Figures 1f–1h) and in the atmosphere. In this context, the relative amount of heavy water, $\delta^{18}O$ in precipitation, serves as a more versatile and effective measure for evaluating the modeled water cycle. This is because $\delta^{18}O$, determined by fractionation processes, is more sensitive to phase change processes than changes in typical water amount, especially in extreme climate conditions like very dry or cold environments.

As shown in Figure 2a (from Group 1), lighter water (lower value of $\delta^{18}O$) travels further from the ocean to inland because heavy water isotopes preferentially condense early in the atmosphere. In the subtropical high-pressure regions that span both oceanic and terrestrial zones, descending air motions result in less precipitation (Figure 1b), offering fewer opportunities for the depletion of atmospheric vapor isotopes by rainfall. However, the isotopic composition of precipitation may differ depending on surface conditions. Over the oceans, heavy isotopes are supplied to the atmosphere through evaporation; hence, when precipitation occurs, it contains a higher concentration of heavy isotopes without previous significant depletion. In contrast, in the desert regions of Africa and Australia, where heavy isotopes are not supplied to the atmosphere via surface evaporation, a pronounced continent effect emerges, leading to precipitation with reduced isotope values.

In the Maritime Continents, the amount effect, which is sensitively tied to deep convection (Tharammal et al., 2017), depletes heavy water. The well-known latitude effect also occurs as moisture moves to cold, high latitudes; its isotope ratio decreases progressively due to Rayleigh fractionation processes (Clark & Fritz, 1997). In regions where these fractionation effects (Dansgaard, 1964) are strong or overlap, such as in high mountains or dry areas like the Sahara Desert, Antarctica, and Greenland (Figure 2e), the spread of modeled $\delta^{18}O$ in precipitation is significant. This is because different models have different cloud physics or convection schemes. However, patterns of spread in $\delta^{18}O$ in precipitation and precipitation amounts (Figure 1f) differ. This is because water vapor $\delta^{18}O$ in the atmosphere can be enriched by re-evaporation or affected by different vapor sources while being modeled in the atmospheric circulation system. Notably, the spread of $\delta^{18}O$ in the atmosphere nudged by different reanalyses (Group 2, Figure 2f) is much smaller than the impact from models (Group 1, Figure 2e).

The second-order parameter in isotopic analysis, known as deuterium excess (abbreviated as d-excess), reflects the characteristics of water source environments (Figures 2c and 2d). It is determined by the local relationship between δD and $\delta^{18}O$. Cold, dry, and land-sourced water is known to increase the kinetic fractionation (in humid-deficit non-equilibrium conditions) of evaporation and d-excess values (Craig, 1961; Harmon & Schwarcz, 1981). The modeled d-excess value is notably diverse in the Sahara Desert, irrespective of the model or reanalysis nudging choice, mainly due to deficient precipitation (Figures 2g and 2h). Antarctica is the region with the highest spread of modeled isotope values. Intrinsically, uncertainties in modeled surface temperatures contribute to this spread in $\delta^{18}O$ and d-excess. Moreover, Antarctica's vast, cold, and dry land conditions may make water isotope simulations more sensitive and variable. Conversely, the spreads of $\delta^{18}O$ and d-excess in the precipitation according to the reanalysis choice are much less than the spreads among models (standard deviation for models $\delta^{18}O$: 3.8‰ and d-excess: 11.7‰, and for reanalyses $\delta^{18}O$: 0.9‰ and d-excess: 1.6‰), as shown in Figures 2e and 2g (Group 1) and Figures 2f and 2h (Group 2). Despite the small amount of precipitation in Antarctica, different horizontal resolutions and a lack of polar-specific physics result in precipitation biases in GCMs (Genthon et al., 2009; Tewari et al., 2022), leading to a greater spread of isotope values than the reanalysis forcing difference.

3.1.2. Evaluation of Water Isotopes in Precipitation and Surface Water Vapor From Monthly to Daily Time Scales

The model's capability to simulate water isotopes was evaluated using both in situ and satellite data. The Taylor diagram (Figure 3) presents the model-data correlation for monthly variations in temperature, precipitation, $\delta^{18}O$, and d-excess at the GNIP sites. Points closer to the reference (REF) data indicate higher model-data correlations and more similar standard deviations between the modeled and observed signals.

The nudged temperature showed a high correlation of about 0.9, and the variance of the modeled precipitation was closest to the observations (standardized deviation ~1.0 in the Taylor diagram). For water isotope values in

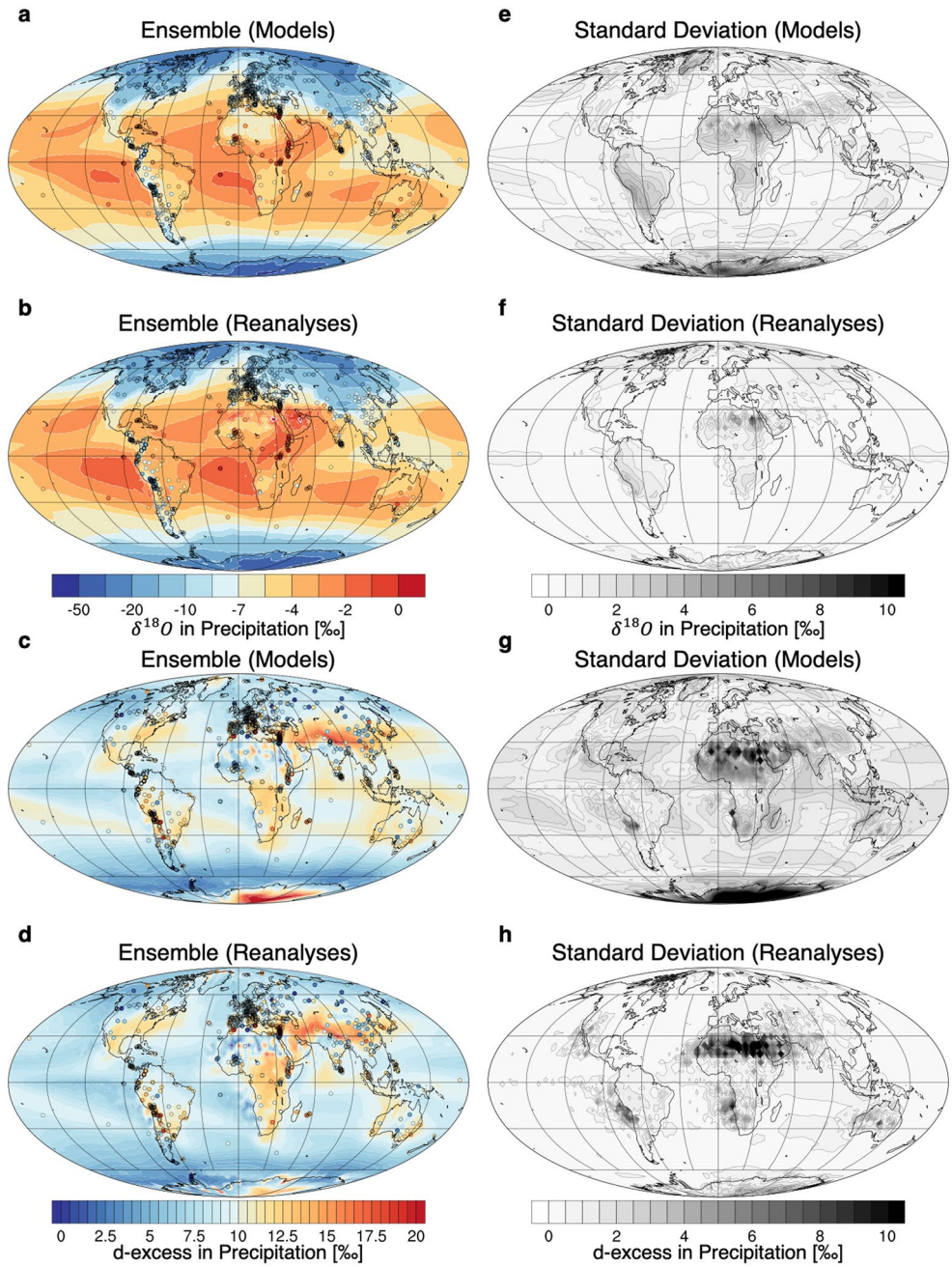

Figure 2. The annual means of ensemble models (a–d) are as follows: (a, c) represent the average of three models from Group 1, which includes IsoGSM.JRA55, MIROC5-iso.JRA55, ECHAM6-wiso.JRA55. Panels (b, d) are based on nudging to three reanalyses from Group 2: IsoGSM.JRA55, IsoGSM.NCEPR2, and IsoGSM.ERA5. The standard deviations for these ensembles (a–d) are represented as (e–h): (e) and (f) for $\delta^{18}O$ (‰ or per mil) and (g, h) for d-excess in precipitation. The colored circles depict the annual mean of the respective Global Network of Isotopes in Precipitation observations.

precipitation, $\delta^{18}O$ tended to follow the precipitation performance; however, the correlation was lower by about 0.1, and its variance was slightly larger (standardized deviation above 1.0) than precipitation. The d-excess parameter presented challenges due to its significantly smaller correlation and larger variance than other variables. This disparity arises from the complexities in accounting for kinetic fractionation during evaporation processes. Moreover, excluding this kinetic process might result in a more unrealistic d-excess during water evaporation from land or when it re-evaporates in the atmosphere.

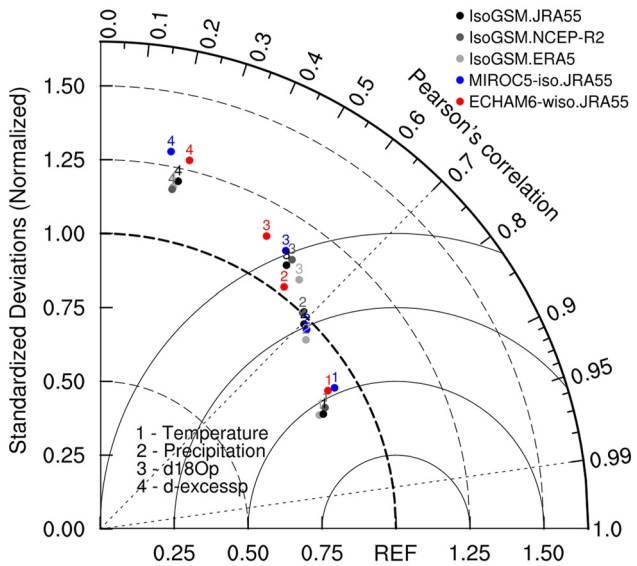

Figure 3. Taylor diagram demonstrates model performance at Global Network of Isotopes in Precipitation (GNIP) sites for monthly mean temperature, precipitation, and isotopic ratio ($\delta^{18}O$ and d-excess) in precipitation, benchmarked against observations from the respective data sets from Climatic Research Unit gridded Time Series (CRU TS) v4.06 near-surface temperature, Global Precipitation Climatology Project v2.3 monthly satellite-gauge combined precipitation, and GNIP, as references. The metrics for assessing performance skill include the averaged Pearson's correlation coefficients and the standardized deviations (represented as the ratio of simulation variance to reference observation variance).

To improve the model-data correlation for isotope values in precipitation, one approach is to create a model ensemble ($\delta^{18}O$, δD, d-excess in Table 2 and Table S1 in Supporting Information S1) using the same reanalysis for nudging (JRA55), which corresponds to Group 1 (IsoGSM.JRA55, MIROC5-iso.JRA55, ECHAM6-wiso.JRA55). In the model ensemble (Mo ENS), precipitation (GNIP) and surface water vapor (SWVID) isotope observations were always better correlated than with the individual models. In the case of $\delta^{18}O$, the global mean correlation value with GNIP data (0.601) was similar to that of the SWVID data set (0.570). One aspect to note is that the GNIP sites are densely located in the European region (Figure 4), so correlations in SWVID data cannot be directly compared due to the differences in time resolution and seasonality across various areas.

When considering the same model (Group 2 using IsoGSM), the correlation between observation and simulation nudged to ERA5 was higher than that achieved using other reanalyses for nudging. On a regional scale, selecting the appropriate reanalysis data set for nudging becomes crucial and depends on the targeted area (Table S2 in Supporting Information S1). For instance, between 60° north and the pole, the dynamics of JRA55, such as temperature and wind fields, correlate best with isotopic observations. Specifically, between 30° and 60° north, JRA55 for nudging is the most suitable for explaining temporal variation in Eastern North America (0.588) and Western Eurasia (0.396). However, its performance declines in Eastern Eurasia (0.275) due to the influence of a strong, wavering jet stream, which leads to highly variable precipitation in the mid-latitudes of the Northern Hemisphere. In Antarctica, the worst reanalysis choice (NCEP-R2) for nudging IsoGSM, in terms of the evaluation of modeled water isotopes at the global scale, resulted in the highest model-data correlations (0.930) and regression slopes (0.74) closest to 1 with the Antarctic snow data set. Thus, a better regional-scale analysis for water isotope studies requires careful selection of the nudging reanalysis data set.

3.2. Atmospheric Variables

3.2.1. Mean Conditions and Atmospheric Moisture Cycling Between Ocean and Land

In the water cycle, water vapor absorbs surplus solar heat and is transported from the tropics toward the poles through meridional eddy moisture transport, and from the ocean to land, releasing heat into energy-deficient regions with variations depending on the hemisphere (Figure 5a). Processes that result in fractionation, such as the amount effect in the Maritime Continents, the continental effect from seacoasts to inland areas, and the altitude effect in mountains and plateaus, influence the isotopic composition of water vapor (Figure 5b).

In all oceans, a subtropical high-pressure system increases evaporation minus precipitation by surface winds and inhibits the uplift of air mass. This keeps heavy water in the atmosphere without being removed by rainfall. Also, western boundary currents play a crucial role in shaping the hemispheric contrast of the water isotope distribution. These narrow and fast meridional currents transports heat energy poleward and release energy through latent heat and water vapor into the atmosphere that becomes dry from mid to high latitudes. In a dry atmosphere above the ocean, particularly where the air sinks in the mid-latitudes, the Northern Hemisphere ends up being wetter than the Southern Hemisphere, highlighting different roles in water transportation toward the poles.

As the water moves from the humid equator toward drier high latitudes, the observed water vapor concentration and its isotopic composition vary between the Northern and Southern Hemispheres due to differences in the spatial coverage of land (Figure 5c). In latitudes between 20° and 60°, the Northern Hemisphere has more land coverage, which places the source of water vapor further away. In contrast, the expansive Southern Ocean supplies abundant water to the land and drives a more extensive water cycle compared to the Northern Hemisphere. As a result, the atmosphere over the northern continents is significantly drier than that over the southern continents.

Table 2
The Global Average of Pearson's Correlation Coefficient Is Calculated From Model Simulations, Which Include Ensembles for Models (Mo ENS, Group 1) and Different Reanalyses (Re ENS, Group 2)

	GSM JRA55	GSM NCEPR2	GSM ERA5	GSM Re ENS	MIROC5 JRA55	ECHAM6 JRA55	Mo ENS JRA55
Global network of isotopes in precipitation (GNIP)/precipitation/monthly							
2m Temp (CRU)	0.889*	0.880**	0.887*	0.896	0.856*	0.854	0.894
Precip (GPCP)	0.705*	0.683*	0.735**	0.742	0.718**	0.605	0.748
$\delta^{18}O$	0.573	0.565	0.612*	0.606	0.561	0.514	0.601
d-excess	0.219	0.207	0.208	0.233	0.184	0.235	0.259
Total average	0.596	0.583	0.611	0.619	0.580	0.552	0.625
Stable water vapor isotope database (SWVID)/hourly/near-surface							
2 m Temp	0.876	0.834	0.879	0.877	0.818	0.839	0.878
2 m S. Humidity	0.726	0.680	0.741	0.737	0.646	0.711	0.755
$\delta^{18}O$	0.504	0.485	0.486	0.511	0.437	0.503	0.570
d-excess	0.085	0.105	0.089	0.108	0.117	−0.001	0.086
Total average	0.546	0.522	0.542	0.554	0.502	0.519	0.583
Database of Antarctic snow isotopic composition/annual mean							
r ($\delta^{18}O$)	0.920	0.930	0.928	0.927	0.924	0.942	0.940
r (d-excess)	0.62	0.74	0.63	0.68	0.79	0.85	0.82

Note. The observations used for validation are water isotopes from the monthly Global Network of Isotopes in Precipitation (GNIP), hourly Stable Water Vapor Isotope Database (SWVID), and the annual mean Database of Antarctic snow isotopic composition. In GNIP sites, values marked with a single asterisk "*" indicate a standard deviation within the range of 0.2–0.25, and those marked with a double asterisk "**" indicate a standard deviation below 0.2, with respect to the global distribution. The climate data set for temperature and precipitation at these sites utilizes CRU TS temperature and GPCP precipitation. Additional correlation coefficients can be found in Table S1 in Supporting Information S1.

At the same time, depletion of δD becomes more sensitive to humidity decreases between land and ocean in the higher latitudes because the remaining vapor in the cloud becomes colder, thereby enhancing fractionation through the Rayleigh process (Clark & Fritz, 1997). The models (Figures 5d and 5e) underestimate the amount of atmospheric water vapor compared to the observations (Figure 5c), being 0.69–1.45 mmol/mol lower between 20° and 60° latitudes, and 2.45–3.05 mmol/mol lower in the tropics. However, the models perform well in simulating the hemispheric contrasts of the water vapor concentrations and their isotope ratios. We find significant differences in model spread (measured as the standard deviation of scattered points) in the land-ocean moistening and dehydrating processes on water vapor and δD: 0.16 mmol/mol and 5.64‰ standard deviation over land and 0.22 mmol/mol and 3.75‰ over the ocean. This implies that the modeled heavy water isotope values also exhibit non-negligible uncertainty, particularly when considering the atmosphere over land.

3.2.2. Evaluation of the Atmospheric Isotopic Composition of Water Vapor

We considered the mid-troposphere, which includes the most sensitive levels (825, 681, and 464 hPa) in estimating the TES δD profile (Yoshimura et al., 2011) containing a substantial portion of water vapor in the vertical profile. The temporal correlation of vertically integrated daily δD between observations and simulations is positive from 60°S to 60°N latitude (Figure 6), and simulations nudged to JRA55 and ERA5 perform better (Table S3 in Supporting Information S1 and Figure 7) over the ocean and land, respectively. Overall, these patterns become increasingly apparent as the altitude rises to 464 hPa. The model ensembles of δD come closer to observation (Figures 7b–7d), and the root mean square deviation (RMSD) decreases significantly from 54.94‰ at 825 hPa to 24.36‰ at 464 hPa.

Also, the overall vertically integrated δD values, when considering the three levels' amount of water vapor, reproduce a better time variation of the TES δD than when considering only single levels in the daily climatology of the spatial mean from 60°S to 60°N latitude (correlation = 0.894 in Figure S2a in Supporting Information S1,

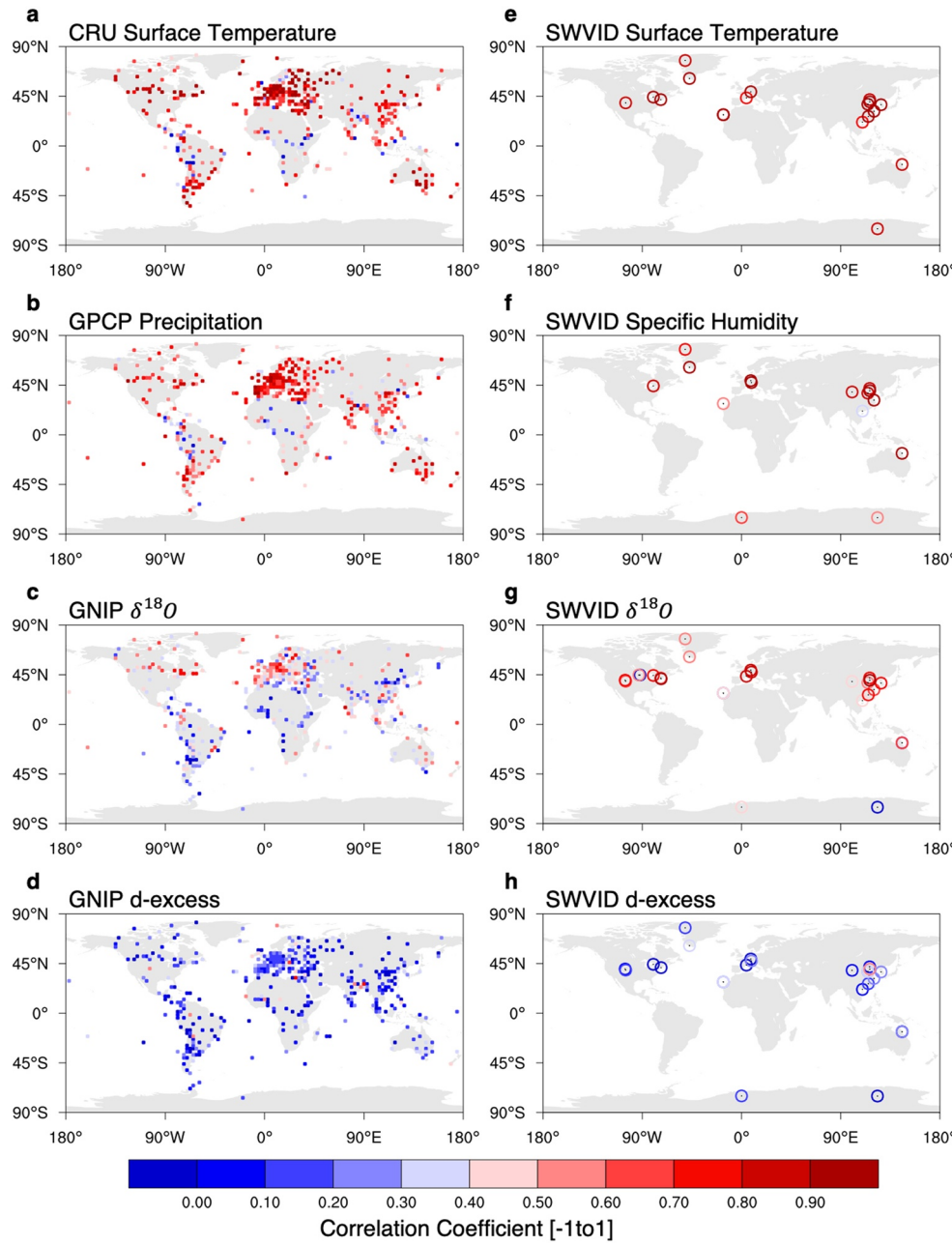

Figure 4. (a–d) Spatial distribution of temporal Pearson's correlation between model ensemble of Group 1 and observations at Global Network of Isotopes in Precipitation (GNIP) station locations for temperature (CRU TS), precipitation (Global Precipitation Climatology Project), $\delta^{18}O$ and d-excess, respectively. GNIP observation data are interpolated to T42 horizontal resolution for model comparison by averaging the values of the points closest to T42 grids. Seasonality is removed in modeled and observed isotope values in GNIP sites to alleviate more substantial seasonal variation in the tropics. Panels (e–h) as for (a–d) but with daily water vapor isotopes data set Stable Water Vapor Isotope Database. The circles are the site locations.

model-data slope = 0.99 in Table S3 in Supporting Information S1). Integrating multiple vertical levels not only offsets the bias but also reduces the negative correlation value in high-latitude regions.

Low correlations are closely related to the temporal variations in humidity. In the tropics, the modeled vertical humidity along the ITCZ seasonal movement range was drier than that in the TES observations (Figure S3b in Supporting Information S1). It becomes even drier from mid to high latitudes due to the cold bias in

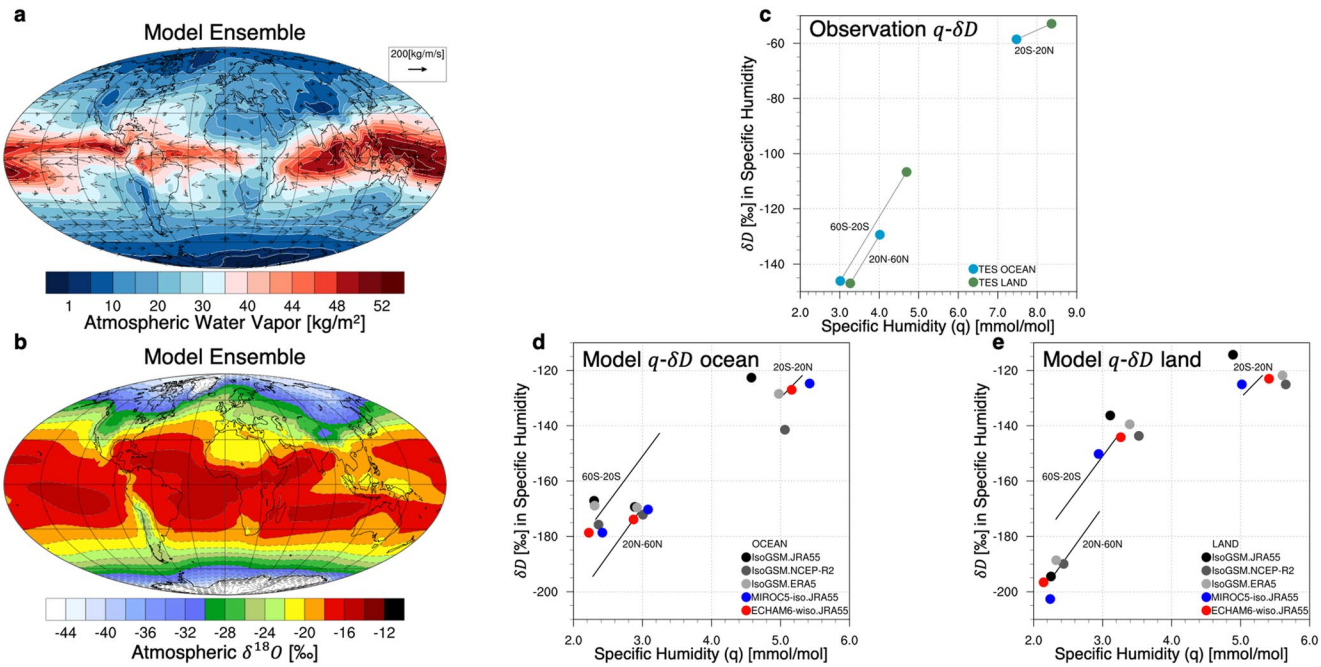

Figure 5. The annual mean of (a) integrated column of water vapor (colored background, kg/m^2) and vertically integrated water vapor transport (kg/m/s) (b) δ^{18}O in the model ensemble of Group 1. Vapor amounts of each pressure thickness are weighted and integrated from 1,000 hPa to 10 hPa. $q-\delta$D pair diagram for moistening and dehydrating process over ocean and land in the collocated annual mean of (c) TES and (d, e) simulations between vertical integrated (825 to 464 hPa) layer in which estimated HDO is primarily sensitive. Black lines connect the average of all simulations' ocean and land in different latitude areas.

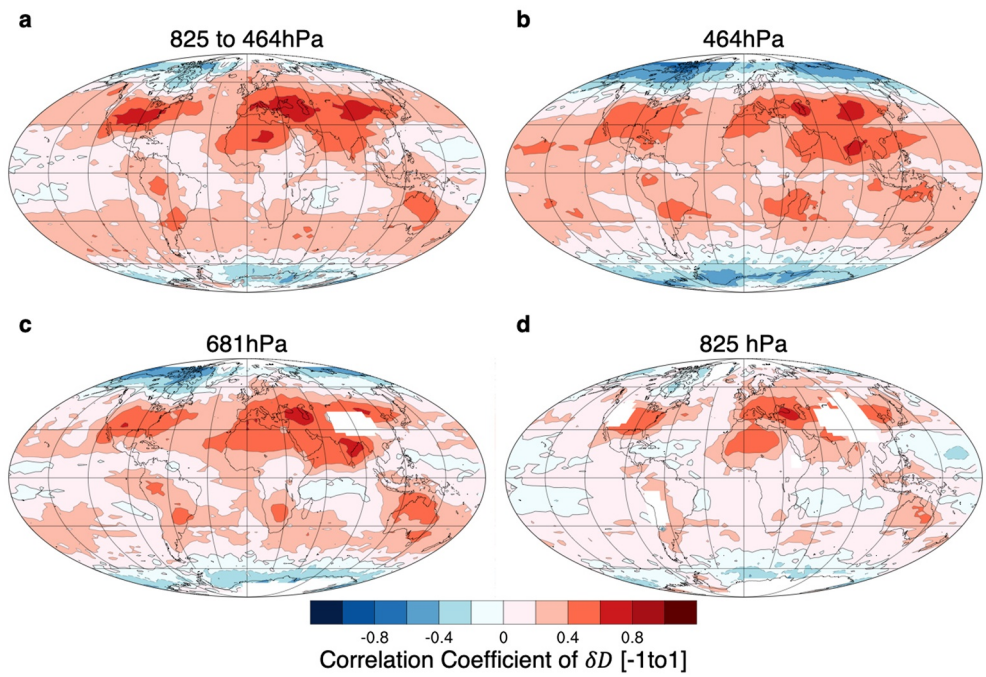

Figure 6. Temporal Pearson's correlation of vertical daily δD between collocated TES and the model ensemble of Group 1 (a) in the vapor amount-weighted integrated column from 825 to 464 hPa, (b) at 464 hPa, (c) at 681 hPa, and (d) at 825 hPa.

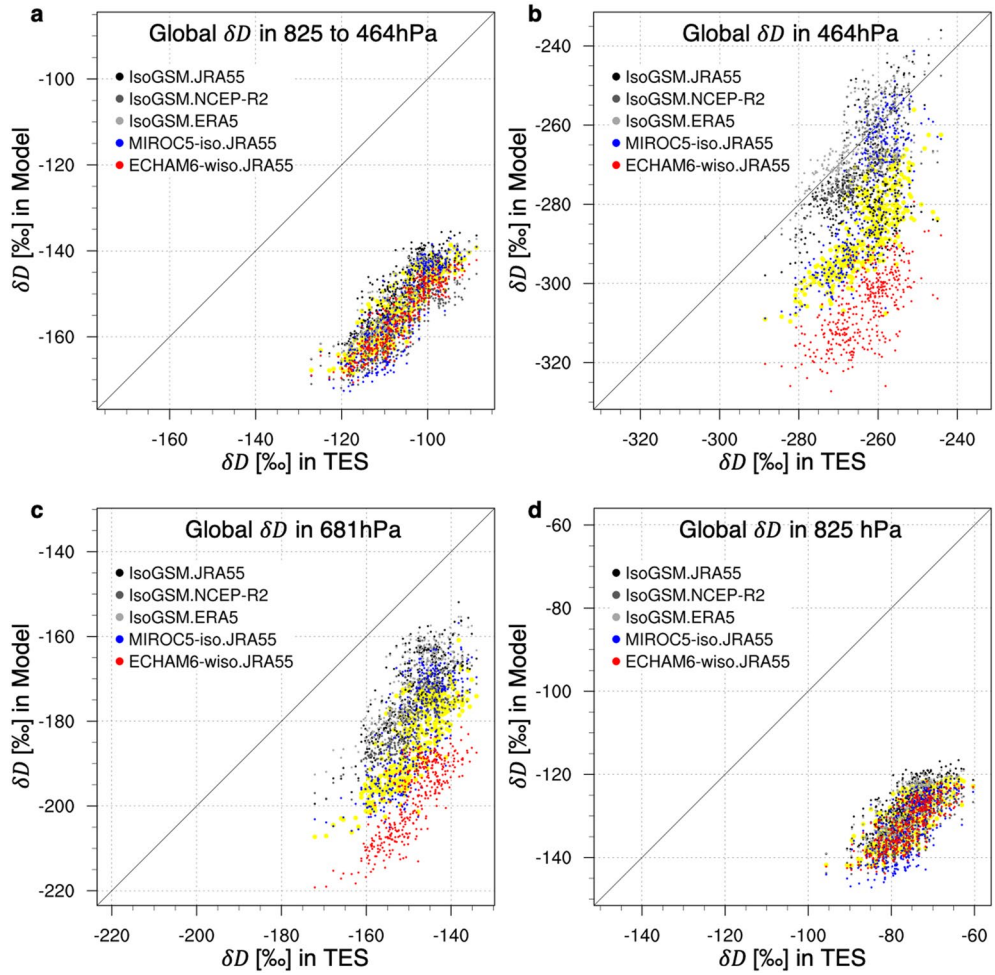

Figure 7. Comparison of global (60°S to 60°N) daily climatology of δD from TES with model ensemble of Group 1 (based on Figure S2a in Supporting Information S1). Plots (a) to (d) are for the integrated column (825–464 hPa) and the 464, 681, and 825 hPa pressure levels, respectively. Yellow scatter points represent the ensemble means of our three models. Multiple-year daily data TES covering from 2004 to 2018 in a non-constant time frame is used to make the annual cycle, and the year 2008 was removed due to a lack of spatial coverage of TES.

the winter hemisphere (Figure S3c in Supporting Information S1). The dryness in the tropics significantly affects the most humid level, 825 hPa, and results in a very large RMSD (70.4‰) and a very low correlation (0.24) in Figure S2c in Supporting Information S1, as seen in Figure 6. The strong cold bias, which causes substantial depletion of δD by decreasing cloud temperature and reducing vapor amount in Figure S3a in Supporting Information S1 in the high latitudes of the winter hemisphere, reduces water vapor by approximately 20%–60% in Figure S3d in Supporting Information S1, especially in Antarctica, and leads to negative correlations.

The difference in the heat capacity between land and ocean influences the correlation of the vertical daily δD with the observations. As humidity over land varies more because of the more extensive changes in daily and seasonal surface temperatures, the temporal correlation is higher in the Northern Hemisphere, which has a more significant proportion of land-covered area. As shown in Figure 6 and Table S3 in Supporting Information S1, the correlation coefficients increased in the order of tropics, Southern Hemisphere, and Northern Hemisphere; correlation over land was higher than over the ocean. As a result, vertically integrated daily δD shows the highest correlation with observations (0.425) in the northern continent and the least in the tropical ocean (0.135). While the land-rich Northern Hemisphere exhibits clearer seasonality and correlates more strongly with observed δD (0.95) than the ocean-rich Southern Hemisphere (0.78), equatorial regions in the model ensemble were found

to vary weakly due to semi-annual cycle influenced by ITCZ north-south migration (Figure S2 in Supporting Information S1). Therefore, the correlation is low (0.47) in the tropics, compounded by the significantly low correlation and high RMSD at the moisture-rich altitude of 825 hPa.

4. Discussion: To What Extent Do Precipitation, Evaporation, and Horizontal Moisture Flux Influence Modeled Atmospheric Water Isotopes?

4.1. Decomposition of Surface-Atmosphere Integrated Budget Analysis

To explain the series of heavy water isotope transports in the water cycle, we utilized an atmospheric water budget analysis to investigate and decompose process-based fractionations. Unlike traditional moisture transport within the water cycle, our method for measuring water isotopic change rate ($\Delta\delta w = \Delta\delta^{18}O‰/day$ in the atmosphere) can help quantify fractionation processes and their proportional contributions. Furthermore, it helps establish the extent to which atmospheric heavy water isotopes are enriched or depleted after evaporation, horizontal moisture flux, and precipitation.

4.1.1. Fractionations Derived by Evaporation, Precipitation, and Horizontal Moisture Flux

Evaporation-derived fractionation enriches the atmosphere by supplying heavy water through the surface-air interface (Figure 8a). This is more pronounced in high-latitude oceans (south: 3.49‰/day, north: 2.81‰/day,

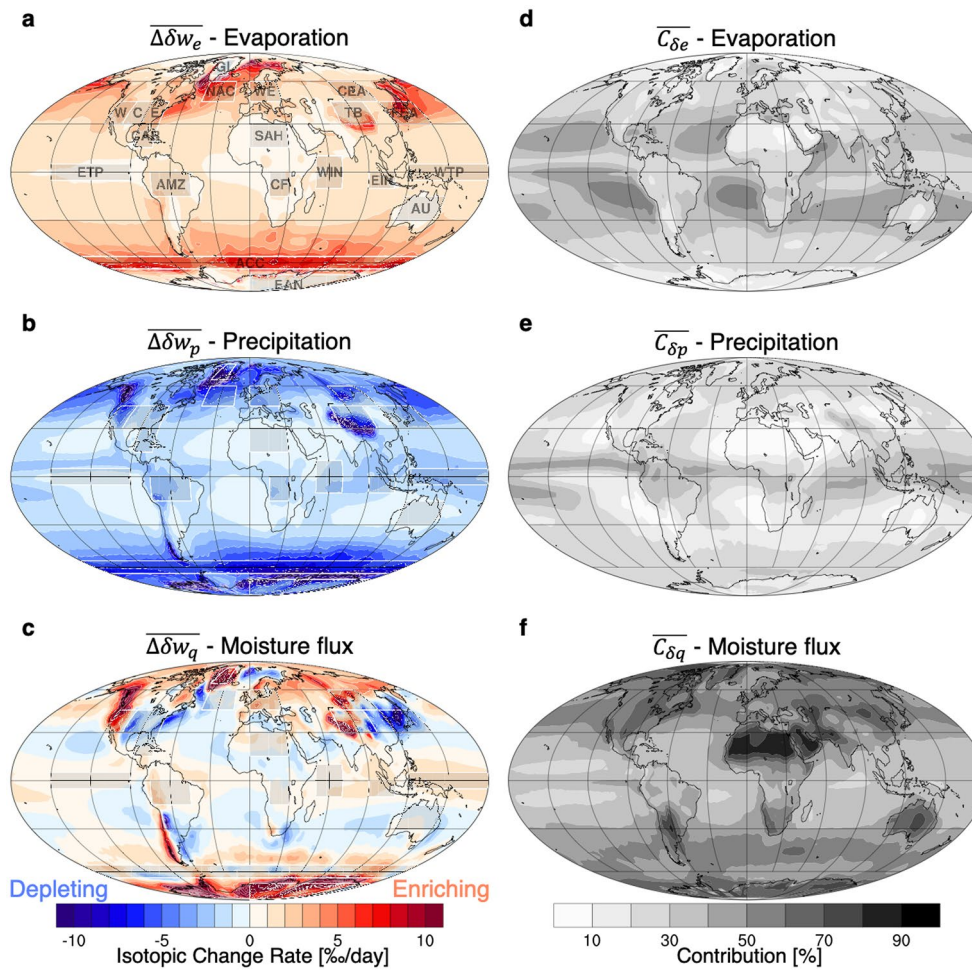

Figure 8. Global time means of decomposed oxygen isotopic change rates in the model ensemble from Group 1, derived from (a) evaporation, (b) precipitation, and (c) horizontal moisture flux. The contributions of decomposed processes are shown in (d) evaporation flux-derived, (e) precipitation flux-derived, and (f) horizontal moisture flux-derived changing $\delta^{18}O$ in the atmosphere.

and tropics: 1.28‰/day in Table S4 in Supporting Information S1), indicating that the gradient of isotope values between the ocean and atmosphere is more prominent, even though the evaporation amount is smaller than in low-latitude oceans. Moreover, the dehydrated marine atmospheric boundary layer in the cold, high-latitude atmospheres is more strongly influenced by warm, moist western boundary currents (Figure 5a).

Precipitation-derived fractionation is also high in high latitudes (south: −4.95‰/day, north: −4.37‰/day, and tropics: −1.66‰/day) due to the Rayleigh fractionation, which increases depletion in the colder cloud (Figure 8b). Other atmospheric fractionation processes related to precipitation, such as the continental effect globally and the altitude effect in high mountains and the Tibetan Plateau, have also been simulated. In tropical oceans, rainfall generates a large amount of precipitable water at the surface (Figure 1b). However, the amount effect is less significant than the other effects mentioned above (average of four tropical regions in India and Pacific Oceans: −1.82‰/day, compared to North Atlantic Current: −5.06‰/day and Antarctic Circumpolar Current: −6.57‰/day). A lower $\Delta\delta w_{p_t}$ implies a smaller gradient of isotope values between surface precipitation (δp_t in Figure 2a) and atmosphere (δw_t in Figure 5b) in the tropics. This is explained by precipitation-derived fractionation term, $\Delta\delta w_{p_t} = -P_t(\delta p_t - \delta w_t)/(W_t + \Delta W_{t\to t+\Delta t})$, as seen in Equation 9 of the isotope mass budget analysis method. In other words, moisture recycling in the tropics occurs more rapidly than in high-latitude regions due to shorter atmospheric water vapor residence time (Gimeno et al., 2021). Consequently, there are fewer chances for the water isotopes to be depleted by precipitation in the tropics. Meanwhile, precipitation-derived highly depleted regions broadly correspond to where moisture converges, such as in Western North America, Tibet, Greenland, and East Antarctica (Figure 8c).

The horizontal gradient of the atmospheric isotope value affects the isotopic change rate induced by fractionation resulting from horizontal moisture transport. The global annual mean of isotopic change rate, which is derived from horizontal moisture flux, is positive, with an average value of $\overline{\Delta\delta w_p} = 1.01‰/\text{day}$. This suggests that atmospheric circulation globally enriches water vapor and alleviates the imbalance between evaporation-derived $\overline{\Delta\delta w_e} = 2.19‰/\text{day}$ and precipitation-derived $\overline{\Delta\delta w_p} = -3.13‰/\text{day}$ isotope change rates (Figure 9 and Table S5 in Supporting Information S1). In other words, the impact of circulation on changes in atmospheric water isotope values is more closely aligned with precipitation's depleting effects rather than evaporation's enriching effects. Indeed, regions that are enriched by circulation tend to correspond with areas that are depleted by precipitation.

4.1.2. Understanding Atmospheric Water Isotope Residuals

Taken together, considering that the atmospheric oxygen isotope residual is small ($\overline{\Delta\delta w} = \overline{\Delta\delta w_e} + \overline{\Delta\delta w_p} + \overline{\Delta\delta w_q} = 0.07‰/\text{day}$, which is equivalent to 1.1% of $|\overline{\Delta\delta w_e}| + |\overline{\Delta\delta w_p}| + |\overline{\Delta\delta w_q}|$), we conclude that isotopic change rates introduced in this study explain a significant feature of large-scale heavy water isotope cycle. As a result, this study has successfully demonstrated that the mass of heavy water remains globally balanced, as indicated by no residual (white bar) in Figure 9a, while providing global estimates for changes in isotopic water rates.

Another approach for understanding the heavy water isotope cycle is to calculate the contributions of the isotopic change rate (Figures 8d–8f). Taking the absolute values of positive enrichment and negative depletion rates and expressing them proportionally in percentages can clarify the contributions of changes in isotope influx and outflux derived by the three different processes. In turn, we can determine which process predominantly determines water isotope values in various regions. The horizontal moisture flux contributes $\overline{C_{\delta q}} = 50.0\%$ of changes in atmospheric isotope value globally, and the contribution of evaporation $\overline{C_{\delta e}} = 27.1\%$ is 4% higher than that of precipitation $\overline{C_{\delta p}} = 22.9\%$ (Table S5 in Supporting Information S1). This is because the evaporation impact occurs over a broad subtropical region (Figure 8d), whereas precipitation mainly controls the isotopic change in the narrow tropical convergence zone (Figure 8e). High-latitude continental water isotopes are more sensitive to horizontal moisture flux (Figure 8f). This accounts for 90% of the isotopic change signal in the vast Sahara Desert, where both precipitation and evaporation are nearly zero.

Strong positive residuals in Greenland and East Antarctica are attributed to similar contributions from horizontal moisture flux (~68%) and precipitation (~22%), which play roles in enrichment and depletion, respectively (Figures 9a and 9b; details in Table S5 in Supporting Information S1). In other words, the positive residuals (white bar) suggest that atmospheric condensation for rain (with its depleting role) does not sufficiently offset the enrichment caused by horizontal moisture flux. However, the mechanisms influencing the residuals in these

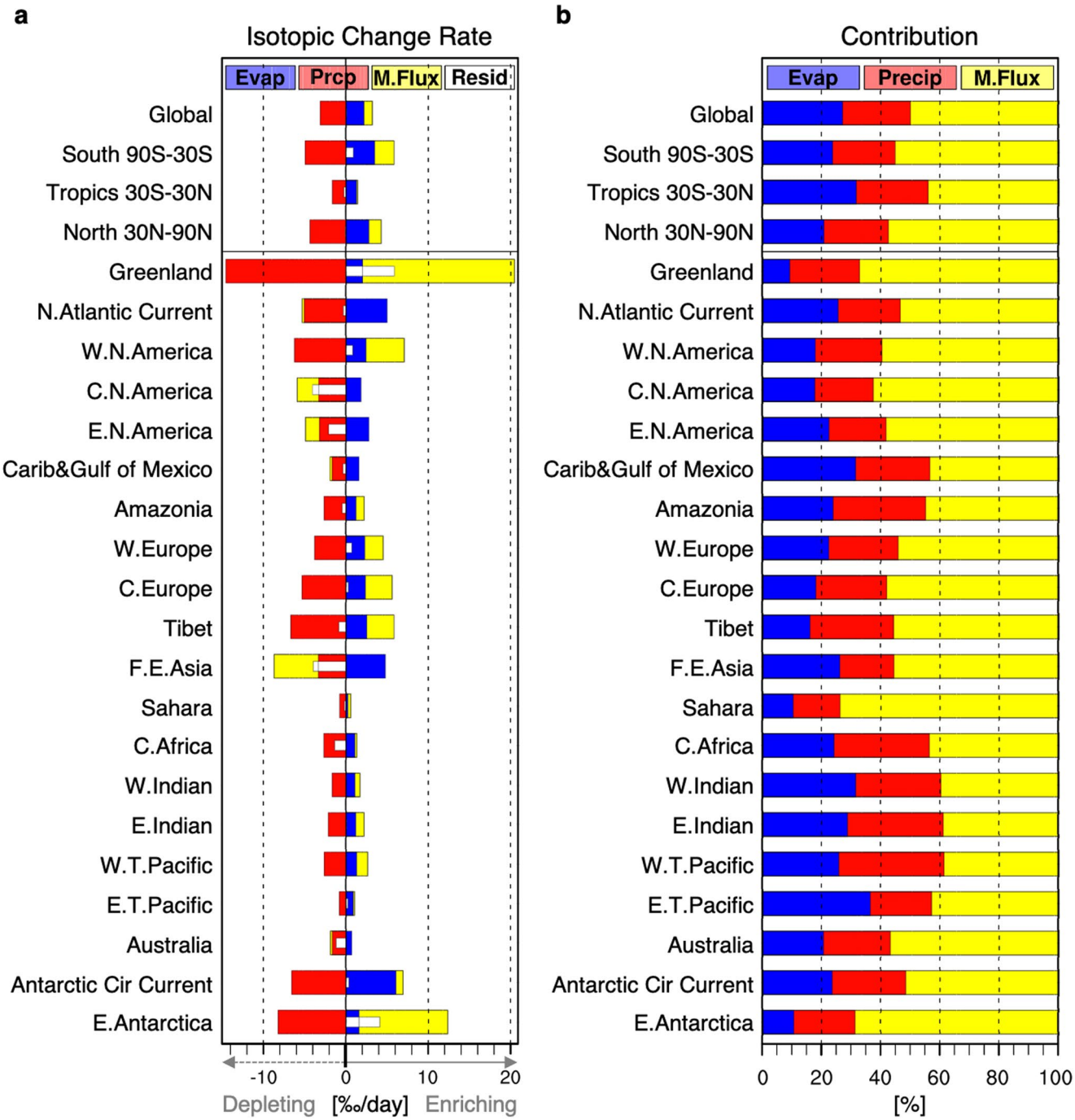

Figure 9. Regional isotope mass budget analysis considering (a) isotopic change rate (‰/day) and (b) relative importance for evaporation, precipitation, and horizontal moisture flux in the model ensemble of Group 1. The white bar ($\Delta\delta w$) represents the residual after considering all isotopic processes ($\Delta\delta w_e + \Delta\delta w_p + \Delta\delta w_q$), indicating whether the water vapor oxygen isotope ($\delta^{18}O$) is depleting or enriching in the atmosphere over the long-term period from 1979 to 2020. The regions are shown in Figure 8a and Figure S4 in Supporting Information S1, and the values are averaged by the areas.

regions differ. The isotopic depletion and enrichment become more pronounced under cold and dry conditions, which are prevalent in these two regions. Moreover, environmental factors such as temperature or relative humidity during evaporation, as well as the distance traveled through dry air, affect precipitation and result in variations in the extent of fractionation changes. In Greenland, the warm North Atlantic Drift transports heat energy to high latitudes, and the newly evaporated oceanic water establishes a more significant horizontal gradient in isotope values. In contrast, in the vast expanse of East Antarctica, fractionations due to phase changes diminish signif-

icantly from the seashore, as water vapor is more likely to condense into precipitation before being transported further inland. Consequently, while the contributions from three isotopic change rates are similar, the rates in Greenland exceed those in Antarctica (details in Table S4 in Supporting Information S1). The positive residuals in the atmosphere also imply that a surplus of isotope residuals can be effectively removed by incorporating more heavy water isotopes once the atmospheric vapor condenses and precipitates. These characteristics have implications for isotope signals recorded in ice cores for past climate studies, especially in Antarctica and Greenland, where annual rainfall is scarce.

In the mid-latitudes, we found substantial negative residuals (white bar in Figure 9a) in Central and Eastern North America and Far East Asia. In these regions, the precipitation-derived isotopic change rate (red bar in Figure 9a) is approximately −3.3‰/day, contributing to about 19.1% of the isotope signal (details in Table S4 in Supporting Information S1). While evaporation depletes (blue bar in Figure 9a), horizontal moisture flux can dampen or enhance atmospheric water isotope differently (yellow bar in Figure 9a). In these regions, it is noteworthy that horizontal moisture flux and precipitation both contribute to decreasing water isotope values in concert (red and yellow bars are all negative), unlike in scenarios where the mechanisms are opposite, such as when increasing moisture due to air convergence leads to decreasing the values due to subsequent rainfall (negative red bar while positive yellow bar). Also, the more significant the contribution of evaporation to the isotopic change rate (Figure 9b), the more horizontal transport depletes heavy water isotopes (Figure 9a). To account for the negative residuals and characteristics observed in these mid-latitude regions, potential mechanisms may involve oceanic vapor sources: westerlies transporting vapor from the ocean to western continents, the polar vortex carrying cold-origin vapor from the Arctic Ocean, and monsoons on the eastern coasts of continents.

In Central North America, the prevailing westerly carries a stream of Pacific Oceanic vapor eastward, enriching water vapor over the western continents and windward coastal mountains (Figures 8b and 8c). Following rainfall, the depleted water vapor isotopes move further east. In Eastern North America and Far East Asia, in winter, a polar vortex allows low-isotope value water originating from the Arctic Ocean to flow into the mid-latitudes. In summer, vapor evaporated from hot and humid western boundary currents, such as the Gulf Stream and Kuroshio Current (Figure 8a), is carried to the east coast under subtropical high pressure (Figure 8c). As a result, the summer monsoon advances northward, bringing increased water vapor isotopes from the evaporation-derived enriched regions to the continents and depleting the atmosphere through horizontal moisture flux-derived fractionation. Similarly, additional water isotope studies can be conducted in various areas to explore different weather and climate change scenarios using this decomposed budget analysis beyond simply focusing on the annual mean analysis.

4.1.3. Exploring Water Source Conditions Through D-Excess Analysis

As a further step, changes in the water source conditions can also be explored by applying our method to d-excess = $\delta D - 8 \times \delta^{18}O$ (Figure S5 in Supporting Information S1). Unlike the isotopic change rates for $\delta^{18}O$, evaporation lower d-excess in the atmosphere (global d-excess ~10‰) by supplying vapor with lower d-excess values originating from the ocean (which are close to zero ‰), as shown in Figure S5a in Supporting Information S1. Similarly, the transport of ocean-oriented water vapor tends to decrease the d-excess over continents, especially in regions where moisture is blocked and converged, such as in the windward coastal Rockies, the Andes Mountains, and Tibet (Figure S5c in Supporting Information S1). All decomposition processes intensify at higher latitudes, owing to increased kinetic fractionation caused by the slower diffusion of $H_2{}^{18}O$ compared to $HD^{16}O$ at lower relative humidity. This results in an excess of D relative to ^{18}O. As a consequence, in dry atmospheric conditions where the slope is lower than 8 (the global meteoric water line) in xy scatter plot (with x representing $\delta^{18}O$ and y representing δD), precipitation-derived depletion causes an increase in the change rate of d-excess at higher latitudes (Figure S5b in Supporting Information S1). Also, it's noteworthy that the contributions from precipitation-derived change rates for d-excess (12.6%) are reduced to half of those for $\delta^{18}O$ (22.9%). This phenomenon arises because equilibrium fractionation becomes dominant during condensation under 100% relative humidity conditions. Specifically, the average contributions are as follows: $\overline{C_{d\text{-excess}_e}} = 23.2\%$, $\overline{C_{d\text{-excess}_p}} = 12.6\%$, and $\overline{C_{d\text{-excess}_q}} = 64.2\%$, while for $\delta^{18}O$, they are $\overline{C_{\delta^{18}O_e}} = 27.1\%$, $\overline{C_{\delta^{18}O_p}} = 22.9\%$, and $\overline{C_{\delta^{18}O_q}} = 50.0\%$. Despite the fact that simulating d-excess poses one of the most formidable challenges in water isotope modeling, our new approach holds the promise of enhancing our comprehension of kinetic fractionation.

4.2. Process-Based Quantification of Uncertainty in Water Isotope Models

Quantifying the uncertainty, which serves as the cause for the spread of modeled variables, provides information about how different water isotopes can be simulated depending on the AGCM used. The modeled spreads of isotopic change rates (represented in brown in Figure 10) are decomposed according to evaporation, precipitation, and horizontal moisture flux, as shown in Figures 11a–11c, respectively.

The moisture flux at high latitudes and mountains accounts for 57% of the total model spread, while precipitation, predominantly on land, accounts for 25% (Figure 10a). Although the same reanalysis is nudged to the models (Group 1), the modeled wind fields carrying moisture flux can vary slightly due to model biases. As such, it is difficult to strictly identify the causes of the spread of moisture flux- and precipitation-derived fractionations. However, they may be influenced by model structural errors caused by schemes for atmospheric transport, convection, or cloud physics. The spreads due to the choice of reanalysis are much smaller than that caused by the model choice (with a ratio of 1:5.6). Although precipitation accounts for 60% (global area average: 0.18‰/day) of the total spread of the three processes (0.30‰/day) resulting from different reanalyses (Group 2), it is smaller than the minor cause, which is evaporation-derived fractionation (0.29‰/day) accounting for 17% of the total spread from the models (1.68‰/day). Upon closer inspection of this global average locally, by averaging the three spreads of processes (Figure 10b), the influence of the model choice is more pronounced in most regions. One exceptional area is the eastern tropical Pacific, where the choice of reanalysis has a more significant impact. Generally, spreads are more prominent where the magnitudes of isotopic change rates are high, such as in Greenland and East Antarctica, at high latitudes. Similar to Tibet and Western North America, some regions in the mid-latitudes also exhibit more significant uncertainty. In such cases, our method can help identify which isotopic fractionation process contributes to higher uncertainty in those regions through regional decomposition analysis (Figures 11d–11f).

In the eastern tropical Pacific region, where air-sea coupling influences El Niño-Southern Oscillation (ENSO), the cause of a larger spread due to reanalysis choice, compared to the models in Figure 10b, is the spread of precipitation-derived fractionation displayed in Figure 11e. This spread (specific values are in Table S4 in Supporting Information S1) is nearly three times larger (0.47‰/day) than that caused by different models (0.16‰/day). Because the physics of the model remains consistent within a single model, reanalyses constrain the large-scale atmospheric circulations differently, affecting factors such as the positions of the ITCZ. This results in differences in atmospheric depletion by precipitation. Therefore, careful attention is required when conducting isotope studies using nudging simulations in the ENSO region, especially when determining precipitation conditions associated with stratus clouds over this area.

Additionally, the Antarctic Circumpolar Current exhibits a notable spread in evaporation-derived fractionation (Figure 11d). This spread is more influenced by variations in sea ice concentration nudging over open seawater than by the choice of model. Specifically, the spread measures 0.67‰/day in simulations from different models in Group 1 and 0.81‰/day in simulations from different reanalyses in Group 2. In the case of Tibet and Western North America, horizontal moisture flux is the most crucial factor contributing to model spread for simulations involving atmospheric water vapor isotopes. Before water isotopes were transported and converged due to atmospheric convergence over Tibet, and before they were transported and converged through atmospheric rivers into Western North America, variations in simulated and transported water vapor within the models (Group 1) can amplify both the spread of precipitable water and the uncertainty in isotopic change rates.

5. Summary and Conclusion

Although numerous comparative studies have been conducted to date, this study presents a unique approach that compared and validated the impact of both models and nudging data on modeled surface and atmospheric water isotopes. Furthermore, it quantified simulation uncertainties in terms of isotopic mass conservation.

With validation against global surface observations, our findings indicate that correlations of modeled isotopes in precipitation and near-surface water vapor are 0.60 for $\delta^{18}O$, while correlations for d-excess are considerably smaller (0.26). Notably, a discernible trend emerged: better performance in simulating temperature, precipitation, and humidity corresponds to higher correlations in modeled water isotope values with observations. However, it is imperative to acknowledge that optimal performance does not always align with specific models or reanalyses for nudging. Consequently, in order to enhance the performance of water cycle simulation, selecting an opti-

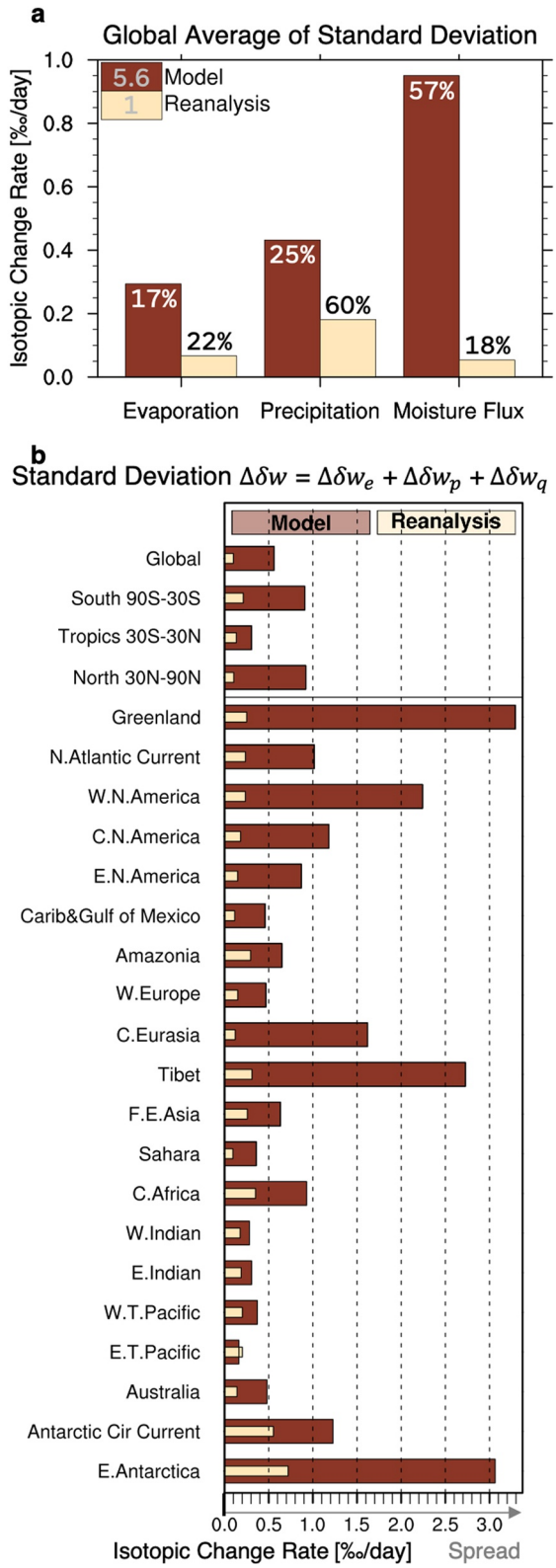

Figure 10. The standard deviation of decomposed isotopic change rate is presented for multiple models (Group 1, represented in brown) and multiple reanalyses (Group 2, represented in lighter color). Global averages of spreads in (a) are from three models and three reanalyses for nudging. Model spread (Group 1) is 5.6 times larger than simulations conducted with different reanalyses (Group 2), and percentages represent proportions to total spread. The bars for uncertainty in (b) present the regional averages of spread for evaporation, precipitation, and horizontal moisture flux, as shown in Figures 11d–11f.

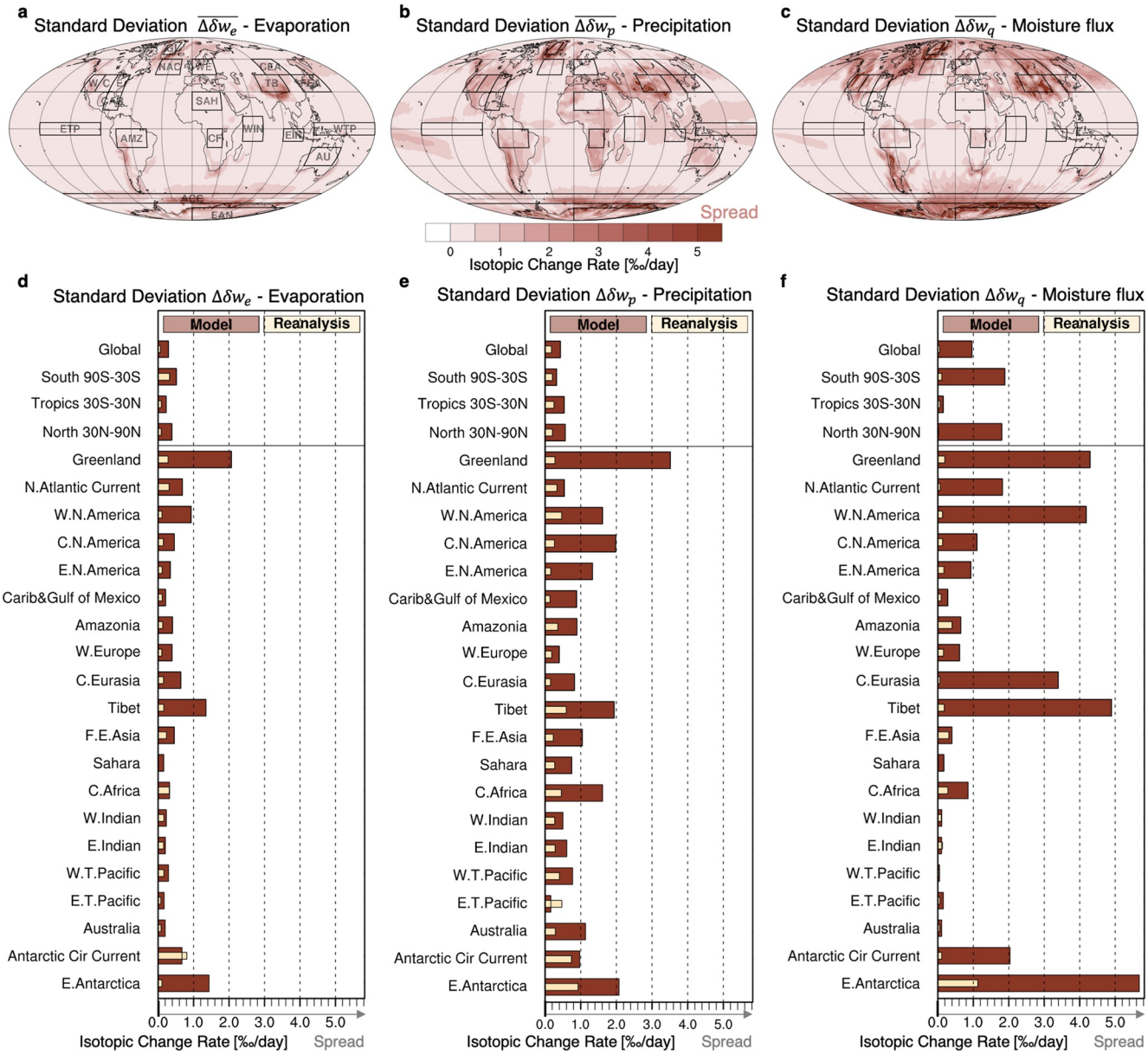

Figure 11. Standard deviation map of decomposed isotopic change rate from multiple models (a) for evaporation, (b) for precipitation, and (c) for horizontal moisture flux. The regional standard deviation of decomposed isotopic change rate from three models (brown for Group 1) and three reanalyses (light color for Group 2): (d) for evaporation from shown in (a, e) for precipitation from (b), and (f) for horizontal moisture flux from (c)

mal combination requires comparing the effects of different models and reanalyses, depending on the specific phenomena and water phases under investigation.

Another approach proposed to improve simulation performance in this multi-model study involves the calculation of averages. When applied to surface water isotopes such as precipitation and near-surface vapor, this method reduces susceptibility to errors by addressing outliers that arise when one model's simulation significantly deviates from the others. Hence, the ensemble of models provides a more comprehensive explanation for surface water isotopes, underscoring the importance of considering multiple water isotope-enabled models. Additionally, by vertically integrating water vapor isotopes, a more robust correlation emerges in the seasonal cycle of the modeled isotope values compared to considering individual altitude layers.

Furthermore, in addition to averaging results or selecting a combination of a certain model and forcing data, gaining a profound understanding of the uncertainty associated with modeling water isotopes in a specific region of interest remains crucial. In light of this, we propose a method that involves examining the change rates of isotope values (expressed in ‰ per day) for $\delta^{18}O$ and d-excess in the atmosphere. This method facilitates the quantitative breakdown of fractionations during the water cycle, spanning from evaporation to precipitation, thereby enabling the identification of processes contributing to the intermodel spread of modeled water isotopes. Consequently, we conclude that the spread in global simulations of modeled water isotopes, which results from model and reanalysis choices, is primarily driven by modeled moisture flux and precipitation uncertainty. These uncertainties originate from distinct model structures and dynamics, specifically atmospheric circulation.

Importantly, this method enables the decomposition of changes in atmospheric water isotopes into hydrological processes, a task that has been challenging due to the limitations of satellite observations. Through this method, the global estimates presented in this study reveal that surface evaporation (which enriches the atmosphere) and atmospheric precipitation (which depletes the atmosphere) do not offset each other's isotopic changes (specifically, depletion by precipitation outweighs enrichment by evaporation) in the atmosphere. This offers a unique perspective on water isotopic fractionation, deviating from the conventional understanding that evaporation and precipitation are balanced in the natural water cycle. Notably, our budget method explains a novel mechanism, viewed from a water isotope perspective, that leads to an enrichment in the isotopic value of atmospheric water through atmospheric circulation, addressing the disparity between evaporation and precipitation. Our findings have the potential not only to estimate how specific processes have influenced atmospheric water isotopes in response to climate changes but also to analyze isotopic variations in phase change in water. From this perspective, our budget analysis utilizes a process-based isotopic mass balance approach to provide a helpful tool for investigating isotopic signals from various regional to global scales, ranging from short-term weather to long-term climate timescales, and for measuring their uncertainty.

Historically, nearly four decades have passed since the inception of the numerical model for globally simulating atmospheric water isotopes (Joussaume et al., 1984). Recent efforts by various modeling groups aim to elucidate novel and intricate water isotope processes across different time periods, achieved by coupling existing atmospheric models with the ocean or by incorporating isotopic processes on land (Brady et al., 2019; Bühler et al., 2021; Cauquoin et al., 2019; Parker et al., 2021). These endeavors could be further enhanced by considering factors such as soil moisture (Zhou et al., 2021), plants (Beyer et al., 2020), surface water (Marković et al., 2020), and anthropogenic combustion-derived vapor (Xing et al., 2020).

Also, water isotope simulations play a practical role in improving model performance by aiding in the determination of physics-related parameters for cloud and convection processes (Ramos et al., 2022). In this regard, the proposition put forth by the US Climate Variability and Predictability Program (CLIVAR) report (Bailey et al., 2021), as well as the perspective shared by S. G. Dee et al. (2023), underscores the significant benefits of incorporating water isotope physics into the physics of Intergovernmental Panel on Climate Change (IPCC)-class GCMs. This integration stands to substantially advance the model, particularly by introducing an observable tracer, water isotopes, that can effectively constrain model physics. Thus, in the context of modeling collaborations, such as the Coupled Model Intercomparison Project or Paleoclimate Modeling Intercomparison Project, the project SWING2, which provides results from water isotope models, has been very useful and important in terms of explaining a large number of observations, enabling the selection of the most appropriate modeling results, and presenting a wide range of modeling outputs to overcome model uncertainties.

Nevertheless, it's important to acknowledge that comprehensive discussions with diverse modeling groups are lacking, and a consensus has yet to be established for a collaborative framework design. Such a design, tentatively termed iso-CMIP or iso-PMIP, can pave the way for future collaborative efforts to improve climate models and analyze the water cycle using the water isotope, a tracer sensitive to changes such as temperature and humidity. Although this study lays the groundwork necessary for a full-scale SWING3, it does not encompass all the existing water isotope-enabled climate models, which include ECHAM (Hoffmann et al., 1998), GENESIS (Mathieu et al., 2002), GISS ModelE (Schmidt et al., 2005), REMOiso (Sturm et al., 2005), DHARMA (Smith et al., 2006), IsoGSM (Yoshimura et al., 2008) HadCM (Tindall et al., 2009), LMDZ-iso (Risi et al., 2010), Isotope-enabled SAM (Blossey et al., 2010), MIROC (Kurita et al., 2011), COSMOiso (Pfahl et al., 2012), ISOLES (X. Lee et al., 2012), UVic (Brennan et al., 2012), iLOVECLIM (Roche, 2013), SPEEDY-IER (S. Dee et al., 2015), Isotope-enabled WRF (Moore et al., 2016), MPI-ESM-wiso (Cauquoin et al., 2019), iCESM (Brady et al., 2019).

Moving forward, it would be advantageous for future full-scale SWING3 projects to prioritize uniform experimental designs, similar to those introduced in this study, by using the same input and experimental framework. Such standardization could enhance both the rigor and interpretability of inter-model comparisons, especially when addressing the challenges of historical climate reconstructions and forward-looking climate simulations. A focused examination of the detailed differences in the models, particularly in their physical components, is also crucial. This would refine our understanding of the uncertainties among models but would also contribute significantly to the robustness of SWING3 project outcomes. Additionally, the budget analysis introduced in this study will help clarify the uncertainty associated with modeled water isotopes.

Particularly, amidst the growing impact of global warming, water isotope modeling emerges as a crucial tool in addressing responses to extreme weather events in the climate change crisis. Moving beyond traditional water isotope modeling for past reconstructions and proxies, studies that focus on understanding water isotopic behaviors under high-moisture conditions, such as during flood events or atmospheric extremes, offer vital insights for disaster preparedness. Through a collaborative, multi-model approach, nudging simulations can tightly constrain atmospheric circulation by leveraging the same present-day reanalysis data, reflecting recent temperature increases. This approach facilitates a more rigorous comparison of hydrological and physical processes simulated in each model, leading to a better grasp of their strengths and weaknesses in simulating water isotopic signals, which are sensitively responded to by changes in climate and weather. The enhanced comprehension of the simulated water cycle not only drives significant advancements in model accuracy but also plays a pivotal role in improving the precision of current-time extreme event predictions through a collaborative ensemble approach involving these refined models.

Data Availability Statement

The modeled water isotopes used for comparison in this study are available at https://isotope.iis.u-tokyo.ac.jp/~hayoung/DATAPUB/2023_Intercomparison/datainfo_README. The initial version is from 1979 to 2020, and the period will be extended.

Acknowledgments

The authors extend their gratitude to the editor, Dr. Yongyun Hu, and the three anonymous reviewers, whose insightful comments and thoughtful suggestions have significantly enhanced the quality of this study. The authors are also very thankful to all precious observational meteorological and water isotope data set providers. All of the data sets used in this study are accessible through the web links provided in the References. This research was supported by the Japan Society for the Promotion of Science, JSPS, (Grants 22H04938 and 21H05002), and the Ministry of Education, Culture, Sports, Science and Technology program, MAXT, for the advanced studies of climate change projection, SENTAN, (Grant JPMXD0722680395), and Advanced practice of watershed flood management using surface hydrological prediction system, "New Social Challenges" mission area, JST-Mirai Program, (Grant JPMJMI21I6), and the Environment Research and Technology Development Fund S-20 (Grant JPMEERF21S12020) of the Environmental Restoration and Conservation Agency of Japan, and Arctic Challenge for Sustainability II, ArCS II, (Grant JPMXD1420318865).

References

Adler, R., Wang, J., Sapiano, M., Huffman, G., Bolvin, D., Nelkin, E., et al. (2017). Global precipitation climatology project (GPCP) climate data record (CDR), version 1.3 (daily) [Dataset]. NOAA National Centers for Environmental Information. https://doi.org/10.7289/V5RX998Z

Adler, R., Wang, J., Sapiano, M., Huffman, G., Chiu, L., Xie, P. P., et al. (2016). Global precipitation climatology project (GPCP) climate data record (CDR), version 2.3 (monthly) [Dataset]. NOAA National Centers for Environmental Information. https://doi.org/10.7289/V56971M6

Aemisegger, F., Pfahl, S., Sodemann, H., Lehner, I., Seneviratne, S. I., & Wernli, H. (2014). Deuterium excess as a proxy for continental moisture recycling and plant transpiration. *Atmospheric Chemistry and Physics*, *14*(8), 4029–4054. https://doi.org/10.5194/acp-14-4029-2014

Bailey, A., Noone, D., Cobb, K., Atwood, A., Dee, S., & Nusbaumer, J. (2021). Water isotopes and climate. A US CLIVAR report. *US Climate Variability and Predictability Program*, *2021*(1), 41. https://doi.org/10.5065/rmyf-qw78

Baker, A., Hartmann, A., Duan, W., Hankin, S., Comas-Bru, L., Cuthbert, M. O., et al. (2019). Global analysis reveals climatic controls on the oxygen isotope composition of cave drip water. *Nature Communications*, *10*(1), 2984. https://doi.org/10.1038/s41467-019-11027-w

Beyer, M., Kühnhammer, K., & Dubbert, M. (2020). In situ measurements of soil and plant water isotopes: A review of approaches, practical considerations and a vision for the future. *Hydrology and Earth System Sciences*, *24*(9), 4413–4440. https://doi.org/10.5194/hess-24-4413-2020

Blossey, P. N., Kuang, Z., & Romps, D. M. (2010). Isotopic composition of water in the tropical tropopause layer in cloud-resolving simulations of an idealized tropical circulation. *Journal of Geophysical Research*, *115*(D24), D24309. https://doi.org/10.1029/2010JD014554

Brady, E., Stevenson, S., Bailey, D., Liu, Z., Noone, D., Nusbaumer, J., et al. (2019). The connected isotopic water cycle in the Community Earth System Model version 1. *Journal of Advances in Modeling Earth Systems*, *11*(8), 2547–2566. https://doi.org/10.1029/2019MS001663

Brennan, C. E., Weaver, A. J., Eby, M., & Meissner, K. J. (2012). Modelling oxygen isotopes in the University of Victoria Earth system climate model for pre-industrial and last Glacial Maximum conditions. *Atmosphere-Ocean*, *50*(4), 447–465. https://doi.org/10.1080/07055900.2012.707611

Bühler, J. C., Roesch, C., Kirschner, M., Sime, L., Holloway, M. D., & Rehfeld, K. (2021). Comparison of the oxygen isotope signatures in speleothem records and iHadCM3 model simulations for the last millennium. *Climate of the Past*, *17*(3), 985–1004. https://doi.org/10.5194/cp-17-985-2021

Cauquoin, A., & Werner, M. (2021). High-resolution nudged isotope modeling with ECHAM6-wiso: Impacts of updated model physics and ERA5 reanalysis data. *Journal of Advances in Modeling Earth Systems*, *13*(11), e2021MS002532. https://doi.org/10.1029/2021MS002532

Cauquoin, A., Werner, M., & Lohmann, G. (2019). Water isotopes–climate relationships for the mid-Holocene and preindustrial period simulated with an isotope-enabled version of MPI-ESM. *Climate of the Past*, *15*(6), 1913–1937. https://doi.org/10.5194/cp-15-1913-2019

Chang, E., & Yoshimura, K. (2015). A semi-Lagrangian advection scheme for radioactive tracers in the NCEP Regional Spectral Model (RSM). *Geoscientific Model Development*, *8*(10), 3247–3255. https://doi.org/10.5194/gmd-8-3247-2015

Chikira, M. (2004). *A numerical study on the green Sahara during the mid-Holocene: An impact of convection originating above boundary layer* (Ph.D. thesis). The University of Tokyo.

Chikira, M., & Sugiyama, M. (2010). A cumulus parameterization with state-dependent entrainment rate. Part I: Description and sensitivity to temperature and humidity profiles. *Journal of the Atmospheric Sciences*, *67*(7), 2171–2193. https://doi.org/10.1175/2010JAS3316.1

Clark, I. D., & Fritz, P. (1997). *Environmental isotopes in hydrogeology*. CRC Press. https://doi.org/10.1201/9781482242911
Conroy, J. L., Cobb, K. M., & Noone, D. (2013). Comparison of precipitation isotope variability across the tropical Pacific in observations and SWING2 model simulations. *Journal of Geophysical Research: Atmospheres*, *118*(11), 5867–5892. https://doi.org/10.1002/jgrd.50412
Craig, H. (1961). Isotopic variations in meteoric waters. *Science*, *133*(3465), 1702–1703. https://doi.org/10.1126/science.133.3465.1702
Craig, H., & Gordon, L. I. (1965). Deuterium and oxygen 18 variations in the ocean and the marine atmosphere, stable isotopes in oceanographic studies and paleotemperatures E. In E. Tongiori (Ed.), *Paper presented at the proceedings of the third Spoleto conference, Spoleto, Italy* (pp. 9–130).
Dansgaard, W. (1964). Stable isotopes in precipitation. *Tellus*, *16*(4), 436–468. https://doi.org/10.1111/j.2153-3490.1964.tb00181.x
Dee, D. P., & Uppala, S. (2009). Variational bias correction of satellite radiance data in the ERA-Interim reanalysis. *Quarterly Journal of the Royal Meteorological Society: A Journal of the Atmospheric Sciences, Applied Meteorology and Physical Oceanography*, *135*(644), 1830–1841. https://doi.org/10.1002/qj.493
Dee, S., Noone, D., Buenning, N., Emile-Geay, J., & Zhou, Y. (2015). SPEEDY-IER: A fast atmospheric GCM with water isotope physics. *Journal of Geophysical Research: Atmospheres*, *120*(1), 73–91. https://doi.org/10.1002/2014JD022194
Dee, S. G., Bailey, A., Conroy, J. L., Atwood, A., Stevenson, S., Nusbaumer, J., & Noone, D. (2023). Water isotopes, climate variability, and the hydrological cycle: Recent advances and new frontiers. *Environmental Research: Climate*, *2*, 022002. https://doi.org/10.1088/2752-5295/accbe1
Derber, J. C., & Wu, W. (1998). The use of TOVS cloud-cleared radiances in the NCEP SSI analysis system. *Monthly Weather Review*, *126*(8), 2287–2299. https://doi.org/10.1175/1520-0493(1998)126%3C2287:TUOTCC%3E2.0.CO;2
Diekmann, C. J., Schneider, M., Knippertz, P., de Vries, A. J., Pfahl, S., Aemisegger, F., et al. (2021). A Lagrangian perspective on stable water isotopes during the West African Monsoon. *Journal of Geophysical Research: Atmospheres*, *126*(19), e2021JD034895. https://doi.org/10.1029/2021JD034895
Dütsch, M., Pfahl, S., Meyer, M., & Wernli, H. (2018). Lagrangian process attribution of isotopic variations in near-surface water vapour in a 30-year regional climate simulation over Europe. *Atmospheric Chemistry and Physics*, *18*(3), 1653–1669. https://doi.org/10.5194/acp-18-1653-2018
ECMWF. (2016a). IFS documentation CY41R2—Part II: Data assimilation. *ECMWF*. https://doi.org/10.21957/vhe0zlxr8
ECMWF. (2016b). IFS documentation CY41R2—Part III: Dynamics and numerical procedures. *ECMWF*. https://doi.org/10.21957/83wouv80
ECMWF. (2016c). IFS documentation CY41R2—Part IV: Physical processes. *ECMWF*. https://doi.org/10.21957/tr5rv27xu
Ek, M. B., Mitchell, K. E., Lin, Y., Rogers, E., Grunmann, P., Koren, V., et al. (2003). Implementation of Noah land surface model advances in the National Centers for Environmental Prediction operational mesoscale Eta model. *Journal of Geophysical Research*, *108*(D22), 8851. https://doi.org/10.1029/2002JD003296
Fiorella, R. P., Poulsen, C. J., & Matheny, A. M. (2018). Seasonal patterns of water cycling in a deep, continental mountain valley inferred from stable water vapor isotopes. *Journal of Geophysical Research: Atmospheres*, *123*(14), 7271–7291. https://doi.org/10.1029/2017JD028093
Gates, W. L. (1992). AN AMS continuing series: Global CHANGE-AMIP: The atmospheric model intercomparison project. *Bulletin of the American Meteorological Society*, *73*(12), 1962–1970. https://doi.org/10.1175/1520-0477(1992)073%3C1962:ATAMIP%3E2.0.CO;2
Genthon, C., Krinner, G., & Castebrunet, H. (2009). Antarctic precipitation and climate-change predictions: Horizontal resolution and margin vs plateau issues. *Annals of Glaciology*, *50*(50), 55–60. https://doi.org/10.3189/172756409787769681
Gimeno, L., Eiras-Barca, J., Durán-Quesada, A. M., Dominguez, F., van der Ent, R., Sodemann, H., et al. (2021). The residence time of water vapour in the atmosphere. *Nature Reviews Earth and Environment*, *2*(8), 558–569. https://doi.org/10.1038/s43017-021-00181-9
Gkinis, V., Vinther, B. M., Popp, T. J., Quistgaard, T., Faber, A., Holme, C. T., et al. (2021). A 120,000-year long climate record from a NW-Greenland deep ice core at ultra-high resolution. *Scientific Data*, *8*(1), 141. https://doi.org/10.1038/s41597-021-00916-9
Harmon, R. S., & Schwarcz, H. P. (1981). Changes of 2H and 18O enrichment of meteoric water and Pleistocene glaciation. *Nature*, *290*(5802), 125–128. https://doi.org/10.1038/290125a0
Harris, I., Osborn, T. J., Jones, P., & Lister, D. (2020). Version 4 of the CRU TS monthly high-resolution gridded multivariate climate dataset [Dataset]. Scientific Data, *7*(1), 109. https://doi.org/10.1038/s41597-020-0453-3
Hayes, J. M. (2004). *An introduction to isotopic calculations*. Woods Hole Oceanographic Institution.
Hersbach, H., Bell, B., Berrisford, P., Hirahara, S., Horányi, A., Muñoz-Sabater, J., et al. (2020). The ERA5 global reanalysis. Copernicus climate change service climate data store (CDS) [Dataset]. Quarterly Journal of the Royal Meteorological Society, *146*(730), 1999–2049. https://doi.org/10.1002/qj.3803
Hoffmann, G., Jouzel, J., & Masson, V. (2000). Stable water isotopes in atmospheric general circulation models. *Hydrological Processes*, *14*(8), 1385–1406. https://doi.org/10.1016/1040-6182(96)00004-3
Hoffmann, G., Werner, M., & Heimann, M. (1998). Water isotope module of the ECHAM atmospheric general circulation model: A study on timescales from days to several years. *Journal of Geophysical Research*, *103*(D14), 16871–16896. https://doi.org/10.1029/98JD00423
Hu, J., Emile-Geay, J., Nusbaumer, J., & Noone, D. (2018). Impact of convective activity on precipitation $\delta^{18}O$ in isotope-enabled general circulation models. *Journal of Geophysical Research: Atmospheres*, *123*(23), 13595–13610. https://doi.org/10.1029/2018JD029187
IAEA/WMO, A. (2006). Global network of isotopes in precipitation [Dataset]. International Atomic Energy Agency/World Meteor-ological Organization. Retrieved from https://nucleus.iaea.org/wiser
Joussaume, S., & Jouzel, J. (1993). Paleoclimatic tracers: An investigation using an atmospheric general circulation model under ice age conditions: 2. Water isotopes. *Journal of Geophysical Research*, *98*(D2), 2807–2830. https://doi.org/10.1029/92JD01920
Joussaume, S., Sadourny, R., & Jouzel, J. (1984). A general circulation model of water isotope cycles in the atmosphere. *Nature*, *311*(5981), 24–29. https://doi.org/10.1038/311024a0
Jouzel, J., Hoffmann, G., Koster, R. D., & Masson, V. (2000). Water isotopes in precipitation:: Data/model comparison for present-day and past climates. *Quaternary Science Reviews*, *19*(1–5), 363–379. https://doi.org/10.1016/S0277-3791(99)00069-4
Juang, H. H. (2007). Semi-Lagrangian advection without iteration. In *Paper presented at the proceedings of the conference on weather analysis and forecasting, central weather Bureau, Longtan, Taoyan, Taiwan*.
Juang, H. H. (2008). Mass conserving and positive semi-Lagrangian tracer advection in NCEP GFS. In *Paper presented at the proceeding conference on weather analysis and forecasting* (pp. 225–227).
Juang, H. H., & Hong, S. (2010). Forward semi-Lagrangian advection with mass conservation and positive definiteness for falling hydrometeors. *Monthly Weather Review*, *138*(5), 1778–1791. https://doi.org/10.1175/2009MWR3109.1
Kanamitsu, M., Ebisuzaki, W., Woollen, J., Yang, S., Hnilo, J. J., Fiorino, M., & Potter, G. L. (2002). NCEP–DOE AMIP-II reanalysis (R-2). NCAR research data archive (RDA). [Dataset]. Bulletin of the American Meteorological Society, *83*(11), 1631–1644. https://doi.org/10.1175/BAMS-83-11-1631

Kanamitsu, M., Kumar, A., Juang, H. H., Schemm, J., Wang, W., Yang, F., et al. (2002). NCEP dynamical seasonal forecast system 2000. *Bulletin of the American Meteorological Society*, *83*(7), 1019–1038. https://doi.org/10.1175/1520-0477(2002)083%3C1019:NDSFS%3E2.3.CO;2

Kobayashi, S., Ota, Y., Harada, Y., Ebita, A., Moriya, M., Onoda, H., et al. (2015). The JRA-55 reanalysis: General specifications and basic characteristics. NCAR Research Data Archive (RDA) [Dataset]. Journal of the Meteorological Society of Japanese Series II, *93*(1), 5–48. https://doi.org/10.2151/jmsj.2015-001

Krabbenhoft, D. P., Bowser, C. J., Anderson, M. P., & Valley, J. W. (1990). Estimating groundwater exchange with lakes: 1. The stable isotope mass balance method. *Water Resources Research*, *26*(10), 2445–2453. https://doi.org/10.1029/WR026i010p02445

Kurita, N., Noone, D., Risi, C., Schmidt, G. A., Yamada, H., & Yoneyama, K. (2011). Intraseasonal isotopic variation associated with the Madden-Julian oscillation. *Journal of Geophysical Research*, *116*(D24), D24101. https://doi.org/10.1029/2010JD015209

Lacour, J., Risi, C., Clarisse, L., Bony, S., Hurtmans, D., Clerbaux, C., & Coheur, P. (2012). Mid-tropospheric δD observations from IASI/MetOp at high spatial and temporal resolution. *Atmospheric Chemistry and Physics*, *12*(22), 10817–10832. https://doi.org/10.5194/acp-12-10817-2012

Lee, J., Fung, I., DePaolo, D. J., & Henning, C. C. (2007). Analysis of the global distribution of water isotopes using the NCAR atmospheric general circulation model. *Journal of Geophysical Research*, *112*(D16), D16306. https://doi.org/10.1029/2006JD007657

Lee, X., Huang, J., & Patton, E. G. (2012). A large-eddy simulation study of water vapour and carbon dioxide isotopes in the atmospheric boundary layer. *Boundary-Layer Meteorology*, *145*(1), 229–248. https://doi.org/10.1007/s10546-011-9631-3

Leng, M. J., & Marshall, J. D. (2004). Palaeoclimate interpretation of stable isotope data from lake sediment archives. *Quaternary Science Reviews*, *23*(7–8), 811–831. https://doi.org/10.1016/j.quascirev.2003.06.012

Lewis, S. C., LeGrande, A. N., Kelley, M., & Schmidt, G. A. (2010). Water vapour source impacts on oxygen isotope variability in tropical precipitation during Heinrich events. *Climate of the Past*, *6*(3), 325–343. https://doi.org/10.5194/cp-6-325-2010

Marković, T., Karlović, I., Perčec Tadić, M., & Larva, O. (2020). Application of stable water isotopes to improve conceptual model of alluvial aquifer in the Varaždin area. *Water*, *12*(2), 379. https://doi.org/10.3390/w12020379

Masson-Delmotte, V., Hou, S., Ekaykin, A., Jouzel, J., Aristarain, A., Bernardo, R. T., et al. (2008). A review of Antarctic surface snow isotopic composition: Observations, atmospheric circulation, and isotopic modeling. PANGAEA [Dataset]. Journal of Climate, *21*(13), 3359–3387. https://doi.org/10.1175/2007JCLI2139.1

Mathieu, R., Pollard, D., Cole, J. E., White, J. W., Webb, R. S., & Thompson, S. L. (2002). Simulation of stable water isotope variations by the GENESIS GCM for modern conditions. *Journal of Geophysical Research*, *107*(D4), 2–18. https://doi.org/10.1029/2001JD900255

Moore, M., Blossey, P. N., Muhlbauer, A., & Kuang, Z. (2016). Microphysical controls on the isotopic composition of wintertime orographic precipitation. *Journal of Geophysical Research: Atmospheres*, *121*(12), 7235–7253. https://doi.org/10.1002/2015JD023763

Moorthi, S., & Suarez, M. J. (1992). Relaxed Arakawa-Schubert. A parameterization of moist convection for general circulation models. *Monthly Weather Review*, *120*(6), 978–1002. https://doi.org/10.1175/1520-0493(1992)120%3C0978:RASAPO%3E2.0.CO;2

Nitta, T., Yoshimura, K., Takata, K., O'ishi, R., Sueyoshi, T., Kanae, S., et al. (2014). Representing variability in subgrid snow cover and snow depth in a global land model: Offline validation. *Journal of Climate*, *27*(9), 3318–3330. https://doi.org/10.1175/JCLI-D-13-00310.1

Nordeng, T. E. (1994). Extended versions of the convective parameterization scheme at ECMWF and their impact on the mean and transient activity of the model in the tropics. In *ECMWF research Department technical memorandum, (206)* (pp. 1–41). https://doi.org/10.21957/e34xwhysw

Nusbaumer, J., & Noone, D. (2018). Numerical evaluation of the modern and future origins of atmospheric river moisture over the West Coast of the United States. *Journal of Geophysical Research: Atmospheres*, *123*(12), 6423–6442. https://doi.org/10.1029/2017JD028081

Okazaki, A., & Yoshimura, K. (2019). Global evaluation of proxy system models for stable water isotopes with realistic atmospheric forcing. *Journal of Geophysical Research: Atmospheres*, *124*(16), 8972–8993. https://doi.org/10.1029/2018jd029463

Oki, T., Musiake, K., Matsuyama, H., & Masuda, K. (1995). Global atmospheric water balance and runoff from large river basins. *Hydrological Processes*, *9*(5-6), 655–678. https://doi.org/10.1002/hyp.3360090513

Onogi, K., Tsutsui, J., Koide, H., Sakamoto, M., Kobayashi, S., Hatsushika, H., et al. (2007). The JRA-25 reanalysis. *Journal of the Meteorological Society of Japanese Series II*, *85*(3), 369–432. https://doi.org/10.2151/jmsj.85.369

Parker, S. E., Harrison, S. P., Comas-Bru, L., Kaushal, N., LeGrande, A. N., & Werner, M. (2021). A data–model approach to interpreting speleothem oxygen isotope records from monsoon regions. *Climate of the Past*, *17*(3), 1119–1138. https://doi.org/10.5194/cp-17-1119-2021

Pfahl, S., Wernli, H., & Yoshimura, K. (2012). The isotopic composition of precipitation from a winter storm—A case study with the limited-area model COSMO iso. *Atmospheric Chemistry and Physics*, *12*(3), 1629–1648. https://doi.org/10.5194/acp-12-1629-2012

Ramos, R. D., LeGrande, A. N., Griffiths, M. L., Elsaesser, G. S., Litchmore, D. T., Tierney, J. E., et al. (2022). Constraining clouds and convective parameterizations in a climate model using paleoclimate data. *Journal of Advances in Modeling Earth Systems*, *14*(8), e2021MS002893. https://doi.org/10.1029/2021MS002893

Risi, C., Bony, S., Vimeux, F., & Jouzel, J. (2010). Water-stable isotopes in the LMDZ4 general circulation model: Model evaluation for present-day and past climates and applications to climatic interpretations of tropical isotopic records. *Journal of Geophysical Research*, *115*(D12), D12118. https://doi.org/10.1029/2009JD013255

Risi, C., Noone, D., Worden, J., Frankenberg, C., Stiller, G., Kiefer, M., et al. (2012). Process-evaluation of tropospheric humidity simulated by general circulation models using water vapor isotopologues: 1. Comparison between models and observations. *Journal of Geophysical Research*, *117*(D5), 1–26. https://doi.org/10.1029/2011JD016621

Roche, D. M. (2013). $\delta^{18}O$ water isotope in the iLOVECLIM model (version 1.0)—Part 1: Implementation and verification. *Geoscientific Model Development*, *6*(5), 1481–1491. https://doi.org/10.5194/gmd-6-1481-2013

Schmidt, G. A., Hoffmann, G., Shindell, D. T., & Hu, Y. (2005). Modeling atmospheric stable water isotopes and the potential for constraining cloud processes and stratosphere-troposphere water exchange. *Journal of Geophysical Research*, *110*, D21. https://doi.org/10.1029/2005JD005790

Shi, X., Risi, C., Li, L., Wang, X., Pu, T., Zhang, G., et al. (2022). What controls the skill of general circulation models to simulate the seasonal cycle in water isotopic composition in the Tibetan Plateau region? *Journal of Geophysical Research: Atmospheres*, *127*(22), e2022JD037048. https://doi.org/10.1029/2022JD037048

Simmons, A. J., Burridge, D. M., Jarraud, M., Girard, C., & Wergen, W. (1989). The ECMWF medium-range prediction models development of the numerical formulations and the impact of increased resolution. *Meteorology and Atmospheric Physics*, *40*(1–3), 28–60. https://doi.org/10.1007/BF01027467

Smith, J. A., Ackerman, A. S., Jensen, E. J., & Toon, O. B. (2006). Role of deep convection in establishing the isotopic composition of water vapor in the tropical transition layer. *Geophysical Research Letters*, *33*(6), L06812. https://doi.org/10.1029/2005GL024078

Sodemann, H., Schwierz, C., & Wernli, H. (2008). Interannual variability of Greenland winter precipitation sources: Lagrangian moisture diagnostic and North Atlantic oscillation influence. *Journal of Geophysical Research*, *113*(D3), D03107. https://doi.org/10.1029/2007JD008503

Stevens, B., Giorgetta, M., Esch, M., Mauritsen, T., Crueger, T., Rast, S., et al. (2013). Atmospheric component of the MPI-M Earth system model: ECHAM6. *Journal of Advances in Modeling Earth Systems*, *5*(2), 146–172. https://doi.org/10.1002/jame.20015

Sturm, K., Hoffmann, G., Langmann, B., & Stichler, W. (2005). Simulation of $\delta^{18}O$ in precipitation by the regional circulation model REMOiso. *Hydrological Processes: International Journal*, *19*(17), 3425–3444. https://doi.org/10.1002/hyp.5979

Takata, K., Emori, S., & Watanabe, T. (2003). Development of the minimal advanced treatments of surface interaction and runoff. *Global and Planetary Change*, *38*(1–2), 209–222. https://doi.org/10.1016/S0921-8181(03)00030-4

Tewari, K., Mishra, S. K., Salunke, P., & Dewan, A. (2022). Future projections of temperature and precipitation for Antarctica. *Environmental Research Letters*, *17*(1), 014029. https://doi.org/10.1088/1748-9326/ac43e2

Tharammal, T., Bala, G., & Noone, D. (2017). Impact of deep convection on the isotopic amount effect in tropical precipitation. *Journal of Geophysical Research: Atmospheres*, *122*(3), 1505–1523. https://doi.org/10.1002/2016JD025555

Thompson, D. M., Conroy, J. L., Konecky, B. L., Stevenson, S., DeLong, K. L., McKay, N., et al. (2022). Identifying hydro-sensitive coral $\delta^{18}O$ records for improved high-resolution temperature and salinity reconstructions. *Geophysical Research Letters*, *49*(9), e2021GL096153. https://doi.org/10.1029/2021GL096153

Tiedtke, M. (1989). A comprehensive mass flux scheme for cumulus parameterization in large-scale models. *Monthly Weather Review*, *117*(8), 1779–1800. https://doi.org/10.1175/1520-0493(1989)117%3C1779:ACMFSF%3E2.0.CO;2

Tindall, J. C., Valdes, P. J., & Sime, L. C. (2009). Stable water isotopes in HadCM3: Isotopic signature of El Niño-southern oscillation and the tropical amount effect. *Journal of Geophysical Research*, *114*(D4), D04111. https://doi.org/10.1029/2008JD010825

Väisänen, A. (1961). Investigation of the vertical air movement and related phenomena in selected synoptic situations. *Commentationes physico-mathematicae/Societas Scientiarum Fennica*, *26*(7), 1–73.

Vitali, V., Martínez-Sancho, E., Treydte, K., Andreu-Hayles, L., Dorado-Liñán, I., Gutierrez, E., et al. (2022). The unknown third–Hydrogen isotopes in tree-ring cellulose across Europe. *Science of the Total Environment*, *813*, 152281. https://doi.org/10.1016/j.scitotenv.2021.152281

Vystavna, Y., Matiatos, I., & Wassenaar, L. I. (2021). Temperature and precipitation effects on the isotopic composition of global precipitation reveal long-term climate dynamics. *Scientific Reports*, *11*(1), 18503. https://doi.org/10.1038/s41598-021-98094-6

Watanabe, M., Suzuki, T., O'ishi, R., Komuro, Y., Watanabe, S., Emori, S., et al. (2010). Improved climate simulation by MIROC5: Mean states, variability, and climate sensitivity. *Journal of Climate*, *23*(23), 6312–6335. https://doi.org/10.1175/2010JCLI3679.1

Wei, Z., Lee, X., Aemisegger, F., Benetti, M., Berkelhammer, M., Casado, M., et al. (2019). A global database of water vapor isotopes measured with high temporal resolution infrared laser spectroscopy [Dataset]. Scientific Data, *6*(1), 1–15. https://doi.org/10.1038/sdata.2018.302

Werner, M., Barras, V., Brown, J., Gourcy, L., Henderson-Sellers, A., Hoffmann, G., et al. (2004). The stable water isotope intercomparison group (SWING)-Results of a new model intercomparison study(Abstract). In *American geophysical union, fall meeting*.

Westerhold, T., Marwan, N., Drury, A. J., Liebrand, D., Agnini, C., Anagnostou, E., et al. (2020). An astronomically dated record of Earth's climate and its predictability over the last 66 million years. *Science*, *369*(6509), 1383–1387. https://doi.org/10.1126/science.aba6853

Worden, J., Bowman, K., Noone, D., Beer, R., Clough, S., Eldering, A., et al. (2006). Tropospheric emission spectrometer observations of the tropospheric HDO/H_2O ratio: Estimation approach and characterization. NASA open data portal [Dataset]. Journal of Geophysical Research, *111*, D16. https://doi.org/10.1029/2005JD006606

Wright, J. S., Sobel, A. H., & Schmidt, G. A. (2009). Influence of condensate evaporation on water vapor and its stable isotopes in a GCM. *Geophysical Research Letters*, *36*(12). https://doi.org/10.1029/2009GL038091

Xing, M., Liu, W., Li, X., Zhou, W., Wang, Q., Tian, J., et al. (2020). Vapor isotopic evidence for the worsening of winter air quality by anthropogenic combustion-derived water. *Proceedings of the National Academy of Sciences*, *117*(52), 33005–33010. https://doi.org/10.1073/pnas.1922840117

Yoshimura, K., Frankenberg, C., Lee, J., Kanamitsu, M., Worden, J., & Röckmann, T. (2011). Comparison of an isotopic atmospheric general circulation model with new quasi-global satellite measurements of water vapor isotopologues. *Journal of Geophysical Research*, *116*(D19), D19118. https://doi.org/10.1029/2011JD016035

Yoshimura, K., Kanamitsu, M., Noone, D., & Oki, T. (2008). Historical isotope simulation using reanalysis atmospheric data. *Journal of Geophysical Research*, *113*(D19), D19108. https://doi.org/10.1029/2008JD010074

Yoshimura, K., Miyazaki, S., Kanae, S., & Oki, T. (2006). Iso-MATSIRO, a land surface model that incorporates stable water isotopes. *Global and Planetary Change*, *51*(1–2), 90–107. https://doi.org/10.1016/j.gloplacha.2005.12.007

Yoshimura, K., Oki, T., Ohte, N., & Kanae, S. (2003). A quantitative analysis of short-term 18O variability with a Rayleigh-type isotope circulation model. *Journal of Geophysical Research*, *108*(D20), 4647. https://doi.org/10.1029/2003JD003477

Zhou, T., Šimůnek, J., & Braud, I. (2021). Adapting HYDRUS-1D to simulate the transport of soil water isotopes with evaporation fractionation. *Environmental Modelling and Software*, *143*, 105118. https://doi.org/10.1016/j.envsoft.2021.105118